Magdalena Bratos
Ryszard Herczyński

THE SHOCK WAVE STRUCTURE IN ONE-COMPONENT GAS AND IN BINARY GAS MIXTURE

19/1983

WARSZAWA 1983

ISSN 0208-5658

Praca wpłynęła do Redakcji dnia 28 września 1982 r.

IPPT PAN

Na prawach rękopisu

Instytut Podstawowych Problemów Techniki PAN
Nakład 160 egz. Ark.wyd. 3,6. Ark.druk.5,25.
Oddano do drukarni w maju 1983 r.
Nr zamówienia 350/83 M-24 .

Warszawska Drukarnia Naukowa, Warszawa,
ul.Śniadeckich 8

M.Bratos, R.Herczyński
Dept. of Fluid Mechanics
Institute of Fundamental Technological Research
Polish Academy of Sciences

THE SHOCK WAVE STRUCTURE IN ONE-COMPONENT GAS AND IN BINARY GAS MIXTURE

Introduction

Experiments made in our laboratory by Walenta,Gmurczyk,Tarczyński [1,2] in xenon-helium mixture following E.Johnson's [3,4] interesting results on the acoustics of mixtures of gases with disparate masses showed an unexpected "hump" at the density shock wave structure. Further investigation with the simultaneous use of two densitometers using different physical principles (electron beam attenuation method and laser differential interferometery) allowed to measure experimentally the separation of gases inside the shock wave and to show that the "hump" mentioned above is connected with the density profile of the lighter component. These experimental observations motivated our interest in this problem.

This paper summarizes our efforts to determine shock wave structures for realistic potentials of Lennard-Jones type using the variational method originated by Tamm [5,6] for monatomic and one-component gas. Tamm used the Mott-Smith distribution function which apparently he invented independently,as a trial distribution function, and obtained the structure of the shock wave in the form of a hyperbolic tangent, similarly as obtained for a weak shock wave by Taylor in 1910 [7]. Tamm's numerical estimations of the shock wave thickness based on the model of hard sphere molecules were obtained for very strong and for very weak shock waves.

To find the shock wave structure in Tamm's approach, calculations of the multiple collision integrals in the Boltzmann equation had to be performed.

As a first step in calculating these integrals we used the model of a two-dimensional gas [8]. Later, a realistic three-dimensional gas was used [9] and these results are also considered here.

In the paper we consider the variational method of solving Boltzmann equations (section 2) showing the forms of functionals, trial functions (generalized Mott-Smith distribution functions) and Euler equations for a single-component gas as well as for a mixture of gases. Section 3 is devoted to the details concerning the calculations of collision integrals; especially, the dynamics of molecular collision is discussed.

The next section (4) is concerned with the numerical characteristics of the shock wave structures. The maximum-slope density thickness is inadequate in the case of mixtures of gases at least with disparate masses, however this definition of thickness can be supplemented by relaxation parameters, which are here considered.

The section 5 concerns the numerical methods used in our calculations. Particularly, we deal with the methods of solving Euler equations obtained in this approach.

Finally, we discuss the results relating to the shock wave structures in a single-component gas (section 6) and in a binary gas mixture (section 7). Special attention is paid to the relation between the dimensionless shock wave thickness and Mach number in front of the shock wave (section 6).

The structures of the shock waves in binary gas mixtures and their properties are discussed in section 7. We consider here the specific structures of the shock waves in binary mixtures of gases with disparate masses. For these mixtures a significant "overshoot" of temperature of the heavy component is noticed.

2. The variational method of solving the Boltzmann equation

In the coordinate system moving with the stationary plane shock wave through the mixture of N noble gases the shock wave is described by the system of Boltzmann equations [6] :

$$(2.1)\quad \underline{c}_i \frac{\partial f_i(\underline{c}_i, x)}{\partial x} = \sum_{j=1}^{N} \int \left[f_i(\underline{c}_i', x) f_j(\underline{c}_{i*}', x) - f_i(\underline{c}_i, x) f_j(\underline{c}_{i*}, x) \right] g_{ij}\, b\, db\, d\varepsilon\, d^3 c_{i*} = \sum_{j=1}^{N} \chi_{ij}(\underline{c}_i, x) \qquad i = 1, 2, \ldots N$$

with the boundary conditions

$$(2.2)\quad f_i(\underline{c}, +\infty) = f_i^+(\underline{c}), \qquad f_i(\underline{c}, -\infty) = f_i^-(\underline{c}),$$

where

$$(2.3)\quad f_i^-(\underline{c}) = n_i m_i^{3/2} (2\pi k T^-)^{-3/2} \exp\left[-m_i (\underline{c} - \underline{v}^-)^2 / 2kT^- \right],$$
$$f_i^+(\underline{c}) = n_i m_i^{3/2} (2\pi k T^+)^{-3/2} \exp\left[-m_i (\underline{c} - \underline{v}^+)^2 / 2kT^+ \right]$$

are Maxwellian distribution functions of the i-th component at $\mp\infty$.

The notation used above is standard: $\underline{c}_i$ and $\underline{c}_{i*}$ (resp. $\underline{c}_i'$ and $\underline{c}_{i*}'$) are velocity vectors of the colliding molecules of the i-th component before (resp. after) a collision, $g_{ij} = |\underline{c}_{i*} - \underline{c}_i|$ is the absolute value of the initial relative velocity, b is the impact parameter and ε is the azimuthal angle.

The integration in (2.1) is performed over the range $0 \le \varepsilon \le 2\pi$, $0 \le b < \infty$ and over the whole three-dimensional velocity space of $\underline{c}_{i*}$.

To obtain the approximate solution of (2.1) the variational method is applied. This method is based on the minimization of the quadratic functional:

(2.4) $$S=\sum_{i=1}^{N}\left\{\int\left[\underline{c}\,\mathrm{grad}\,f_i-\sum_{j=1}^{N}\chi_{ij}\right]^2 d^3c\,dx\right.$$

using trial functions in the form based on the generalized Mott-Smith distribution function [10].

(2.5) $$f_i(\underline{c},x)=\frac{1-h(x)}{2}f_i^-(\underline{c})+\frac{1+h(x)}{2}f_i^+(\underline{c})+\frac{1}{2}\sum_{\substack{j=1\\ j\neq i}}^{N}\beta_{ji}\tilde{h}(x)\left[f_j^+(\underline{c})-f_j^-(\underline{c})\right]$$

$$i=1,2,\ldots\ldots N$$

where $\beta_{ji}=m_j/m_i$ is the ratio of atomic masses.
The auxiliary functions $h(x)$ and $\tilde{h}(x)$ obey the boundary conditions

(2.6) $$h(-\infty)=-1\,,\quad h(+\infty)=1\,,\quad \tilde{h}(-\infty)=\tilde{h}(+\infty)=0$$

The sum on the right hand side of (2.5) describes the influence of all but the i-th component, on the distribution function $f_i(\underline{c},x)$. This influence is proportional to the differences between the appropriate distribution functions of a given gas components at plus and minus infinity.
The chosen form of trial functions (2.5) is the most general function linear with respect to $f_i^+(\underline{c})$ and $f_i^-(\underline{c})$ which automatically fulfils the conservation laws.
The use of trial functions allows to reduce the problem of minimization of the functional S to the solution of the system of two Euler equations for h and $\tilde{h}$. Introducing (2.5) into (2.4) we obtain

(2.7) $$\begin{aligned}S=\int\{&A\,h'^2+A_1h'\tilde{h}'+A_2\tilde{h}'^2+A_3(1-h^2)h'+A_5h\tilde{h}h'+A_6\tilde{h}h'\\&+A_7h'\tilde{h}^2+A_8\tilde{h}'+A_9\tilde{h}'h^2+A_{10}h\tilde{h}\tilde{h}'+A_{11}\tilde{h}\tilde{h}'+A_{12}\tilde{h}'\tilde{h}^2\\&+A_{13}(1-h^2)^2+A_{14}\tilde{h}+A_{15}\tilde{h}^2+A_{16}h\tilde{h}+A_{17}\tilde{h}h^2+A_{18}h\tilde{h}^2\\&+A_{19}\tilde{h}^3+A_{20}\tilde{h}^4+A_{21}\tilde{h}h^2+A_{22}h\tilde{h}^3+A_{23}\tilde{h}^2h^2\}\,dx\end{aligned}$$

where the coefficients A, A_1, ... A_{23} depend on conditions in front of the shock wave and on the intermolecular potential. The dependence of $A, A_1, \ldots A_{23}$ on the conditions behind the shock wave can be eliminated with the use of Rankine-Hugoniot conditions (Appendix A,C). For the mixture of two noble gases these coefficients are listed in the Appendix A.

The system of Euler equations related to (2.7) is

$$
\begin{aligned}
&-2Ah'' - A_1\tilde{h}'' + (2A_9 h - A_5 h + A_{10}\tilde{h} - 2A_4\tilde{h} - A_6)\tilde{h}' - 4A_{13}h + A_{16}\tilde{h} \\
&-2A_{14}h\tilde{h} + A_{18}\tilde{h}^2 + 4A_{13}h^3 - 3A_{16}h^2\tilde{h} + A_{22}\tilde{h}^3 + 2A_{23}h\tilde{h}^2 = 0 \qquad (2.8) \\
&-A_1 h'' - 2A_2\tilde{h}'' + (A_5 h - 2A_9 h + 2A_7\tilde{h} - A_{10}\tilde{h} + A_6)h' + A_{14} \\
&+2A_{15}\tilde{h} + A_{16}h - A_{14}h^2 + 2A_{18}h\tilde{h} + 3A_{19}\tilde{h}^2 + 4A_{20}\tilde{h}^3 - A_{16}h^3 \\
&+3A_{22}\tilde{h}^2 h + 2A_{23}h^2\tilde{h} = 0
\end{aligned}
$$

In this paper the problem of the shock waves propagating either in a pure monatomic gas or in a mixture of two noble gases is considered. In the former case the trial function has the simple form

$$
f(\underline{c}, x) = \frac{1 - h(x)}{2} f^-(\underline{c}) + \frac{1 + h(x)}{2} f^+(\underline{c}) \qquad (2.9)
$$

which is identical with the distribution function introduced by Mott-Smith [10]. This distribution function has been used by Mott-Smith and many others [11-17] first of all in connection with the so called moment method. It should be noted, however, that the use of the variational principle avoids the arbitrariness of selecting moments of the distribution function-necessary in the original Mott-Smith method to complete the set of necessary equations.

The functional (2.4) with the trial function (2.9) has been considered by Tamm [5] for the case of single-component, monatomic gases. He obtained the functional

$$
S = \int \left\{ A h'(x)^2 + B h'(x)\left(1 - h(x)^2\right) + C\left(1 - h(x)^2\right)^2 \right\} dx \qquad (2.10)
$$

where A, B and C are coefficients which depend on conditions in front of the shock wave and on the intermolecular potential. For this functional the Euler equation has the form:

$$h'' + \frac{2C}{A}(1-h^2)\cdot h = 0 \qquad (2.11)$$

and its solution is

$$h(x) = \mathrm{th}\left(x\sqrt{\frac{C}{A}}\right) \qquad (2.12)$$

The Prandtl shock wave thickness Λ related to (2.12) is given by

$$\Lambda = 2\sqrt{\frac{A}{C}} \qquad (2.13)$$

Thus for the determination of the shock wave structure only two coefficients A and C are needed. Tamm [5] found the asymptotic values of A and C for very weak and very strong shock waves.

The expression (2.12) coincides with that found by Taylor for the structure of weak shock waves in a viscous and heat conducting gas in the framework of continuum mechanics.

For an arbitrary intermolecular potential considered here the form of the functional (2.10) remains unchanged and hence also the form of (2.11) - (2.13). Only the coefficient C in (2.12) depends on the intermolecular potential. The formulae for A and C are listed in Appendix A.

3. Dynamics of collisions; collision integrals

In the approach adapted in this paper it is necessary to calculate "collision integrals" (formulae given in Appendix A) for an arbitrary intermolecular potential. The first step in this direction is to express the resulting velocities of colliding molecules (for the assumed intermolecular potential) in terms of their initial velocities and geometrical parameters of the collision, namely the impact parameter b and the azimuthal angle ε.

The collision plane can be defined by coplanar vectors of relative velocities of colliding molecules, $\underline{g}$ and $\underline{g}'$; $\underline{g} = \underline{c}_1 - \underline{c}$,

$\underline{g}' = \underline{c}_{*}' - \underline{c}'$ or - what is more convenient - by $\underline{g}$ and the vector $\underline{k}$ - the unit apse vector -(the vector parallel to the line of symmetry of either trajectory).

On the collision plane the dynamics of collision can be reduced to one body problem [18] . The resulting equations of conservation of energy and of angular momentum in terms of polar coordinate system (r, θ) are (Fig.1):

$$\mu b g = \mu r^2 \dot{\theta}$$

$$\frac{1}{2}\mu g^2 = \frac{1}{2}\mu(\dot{r}^2 + r^2\dot{\theta}^2) + \Phi(r) \tag{3.1}$$

where $\mu = \frac{m_1 m_2}{(m_1 + m_2)}$ is the reduced mass and $\Phi(r)$ is the intermolecular potential.

The resulting relative velocity g' depends on the impact angle Ψ , defined as the value of θ for which the intermolecular separation r is minimum, r_{min} .

From (3.1) one gets

$$\Psi = \int_0^{\pi} d\theta = \int_{-\infty}^{r_{min}} \frac{b/r^2}{\sqrt{1 - \frac{2\Phi(r)}{\mu g^2} - \frac{b^2}{r^2}}}\, dr = \int_0^{\tilde{\beta}_0} \frac{d\tilde{\beta}}{\sqrt{1 - \tilde{\beta}^2 - \frac{2\Phi(b/\beta)}{\mu g^2}}} \tag{3.2}$$

where $\tilde{\beta} = \frac{b}{r}$, $\tilde{\beta}_0 = \frac{b}{r_{min}}$ and r_{min} is the root of the equation $\frac{dr}{d\theta} = 0$.

For $r = r_{min}$ the denominator in (3.2) vanishes and hence the right hand expression has a weak singularity for $\tilde{\beta} = \tilde{\beta}_0$. This singularity can be extracted from the integral (3.2) by transforming it in the form:

$$\Psi = \int_0^{\tilde{\beta}_0} \left\{ \frac{1}{\sqrt{2\tilde{\beta}_0 \tilde{x} - \tilde{x}^2 + \tilde{\Phi}(\tilde{\beta}_0) - \tilde{\Phi}(\tilde{\beta}_0 - \tilde{x})}} - \frac{1}{\sqrt{\tilde{x}(2\tilde{\beta}_0 - \tilde{\Phi}'(\tilde{\beta}_0))}} \right\} d\tilde{x}$$

$$+ \int_0^{\tilde{\beta}_0} \frac{d\tilde{x}}{\sqrt{\tilde{x}(2\tilde{\beta}_0 - \tilde{\Phi}'(\tilde{\beta}_0))}} \tag{3.3}$$

, where $\tilde{\Phi}'(\tilde{\beta}_0) = \frac{d\tilde{\Phi}(\tilde{\beta}_0)}{d\tilde{\beta}_0}$

where $\tilde{x} = \tilde{\beta}_0 - \tilde{\beta}$ and

where $\tilde{\Phi}(\tilde{\beta}) = \frac{2}{\mu g^2} \Phi\left(\frac{b}{\beta}\right)$

The first integral in (3.3) is not singular, the second one can be found analytically.

Now we can express the resulting velocities in an arbitrary fixed system of coordinates (x, y, z) with unit vectors $\underline{e}_x, \underline{e}_y, \underline{e}_z$. The orientation of the collision plane in this system is defined by the azimuthal angle ε. Let the normal unit vector to the collision plane be $\underline{n}_c$, $\underline{n}_c = \frac{\underline{g} \times \underline{k}}{|\underline{g} \times \underline{k}|}$, whereas the unit vector normal to $(x, \underline{g})$ - plane: $\underline{n}_\varepsilon$ is: $\underline{n}_\varepsilon = \frac{\underline{e}_x \times \underline{g}}{|\underline{e}_x \times \underline{g}|}$. The angle between these vectors is $\frac{\pi}{2} - \varepsilon$; thus if $\underline{n}_g$ is the unit vector perpendicular to $\underline{g}$ and lying on the collision plane, $(\underline{n}_g \cdot \underline{g} = 0)$, then $\cos\varepsilon = \underline{n}_g \cdot \underline{n}_\varepsilon$.

The above relations allow to find analytically the vector $\underline{n}_g$ and hence also the vector $\underline{k}$:

$$(3.4) \qquad \underline{k} = \underline{n}_g \sin\Psi + \frac{\underline{g}}{|\underline{g}|} \cos\Psi$$

Finally, the formulae for resulting velocities in the given system of coordinates are:

$$(3.5) \qquad \underline{c}' = \underline{c} + 2\frac{m_2}{m_1 + m_2}(\underline{g} \cdot \underline{k})\underline{k}$$

$$\underline{c}_*' = \underline{c}_* - 2\frac{m_1}{m_1 + m_2}(\underline{g} \cdot \underline{k})\underline{k}$$

Hence, the collision is completely determined by specifying $\underline{c}$, $\underline{c}_*$, ε and Ψ.

For the calculations of multiple integrals $A, A_1, \ldots, A_{25}$ the Monte Carlo method has been used. The velocities of colliding molecules were presented in spherical coordinates

$c_x = c_r \sin\tilde{\theta} \cos\tilde{\omega}$, $c_y = c_r \sin\tilde{\theta} \sin\tilde{\omega}$ and $c_z = c_r \cos\tilde{\theta}$

Thus the calculation of each collision requires eight numbers: $c_r, \tilde{\theta}, \tilde{\omega}, c_{r_*}, \tilde{\theta}_*, \tilde{\omega}_*, \varepsilon, b$ which were uniformly generated

in a hypercube: $0 \le \varepsilon \le 2\pi$, $0 \le \theta, \tilde{\theta}_v \le \pi$, $0 \le \tilde{\omega}, \tilde{\omega}_n \le 2\pi$,

$0 \le b \le b_{max}$, $0 \le c_\tau, c_{\tau'} \le c_{\tau max}$. The values of b_{max}, $c_{\tau max}$ were determined experimentally by analysing the influence of these values on the accuracy of computations. This accuracy was evaluated by comparing the Monte Carlo calculations with analytical values for three integrals: A, A_4, A_5.

For Mach numbers up to $M^- = 4.5 \div 5$ the accuracy of a few percent requires 10^4 pseudorandom numbers. To get the same accuracy for larger Mach numbers it is necessary to use a much greater size sample and the available computer time prevented us to perform calculations for $M^- > 5.0$.

4. Relaxation parameters

The most common numerical characteristic of the shock wave in monatomic gases is its Prandtl's thickness Λ defined by the maximum-slope of density in the shock wave. This definition sometimes supplemented by a parameter describing the asymmetry of the shock wave has been also used for the description of shock waves in gas mixtures. However, as it became clear from the experimental investigations of Gmurczyk et al. [1-2], the structure of the shock wave in mixture of gases at least with disparate masses makes the so defined shock wave thickness inadequate.

Thus an appropriate numerical characteristic for the description of shock waves in mixtures of gases, at last with disparate molecular masses, is required.

We observe that if the shock wave structure is given by (2.12) the value of Λ describes the relaxation process of the shock wave i.e. the way how the gas approaches the equilibrium states at plus and minus infinity. This observation led us to the idea of relaxation parameters for shock waves in binary gas mixtures.

This can be done by finding the asymptotic behaviour of the solution of the Euler equations (2.8).

At $-\infty$ we define the transformation

$$(4.1) \qquad \lambda = \gamma - 1 \quad , \quad \tilde{\lambda} = \tilde{\gamma}$$

which leads to the system

$$-2AY'' - A_1\tilde{Y}'' + \tilde{Y}'[(2A_9 - A_5)Y + (A_{10} - 2A_7)\tilde{Y} + A_5 - A_6 - 2A_9]$$
$$+ 4A_{13}Y^3 - 12A_{13}Y^2 + 8A_{13}Y - 3A_{16}Y^2\tilde{Y} + 2A_{23}\tilde{Y}^2Y + 2(3A_{16} - A_{14})Y\tilde{Y}$$
$$+ 2(A_{14} - A_{16})\tilde{Y} + (A_{18} - 2A_{23})\tilde{Y}^2 + A_{22}\tilde{Y}^3 = 0$$

$$(4.2)\quad -A_1Y'' - 2A_2\tilde{Y}'' - Y'[(2A_9 - A_5)Y + (A_{10} - 2A_7)\tilde{Y} + A_5 - A_6 - 2A_9]$$
$$+ 2(A_{14} - A_{16}) + (3A_{16} - A_{14})Y^2 - A_{16}Y^3 + 2A_{23}Y^2\tilde{Y}$$
$$+ 2(A_{18} - 2A_{23})Y\tilde{Y} + 3A_{22}\tilde{Y}^2Y + 2(A_{15} - A_{18} + A_{23})\tilde{Y} + 3(A_{13} - A_{22})\tilde{Y}^2$$
$$+ 4A_{20}\tilde{Y}^3 = 0$$

The asymptotic behaviour of (2.12) suggests an exponential behaviour of the solution of (4.2) and hence we assume

$$(4.3)\quad Y = a_1 \exp(2\alpha_1 x) \quad , \quad \tilde{Y} = \tilde{a}_1 \exp(2\tilde{\alpha}_1 x)$$

where $a_1, \tilde{a}_1, \alpha_1, \tilde{\alpha}_1$ are constants. The behaviour at infinity depends on linear (with respect to $e^{2\alpha_1 x}$ and $e^{2\tilde{\alpha}_1 x}$) terms and from the linearized system of equations (4.2) we obtain:

$$(4.4)\quad \alpha_1 = \tilde{\alpha}_1 = \frac{1}{2}\sqrt{\frac{-B_1 + \sqrt{B_1^2 - 4B_0B_2}}{2B_0}}$$

where

$$B_0 = 4AA_2 - A_1^2$$

$$(4.5)\quad B_1 = -16A_{13}A_2 - 4A(A_{15} - A_{18} + A_{23}) + 4A_1(A_{14} - A_{16}) + (A_5 - A_6 - 2A_9)^2$$

$$B_2 = -4(A_{14} - A_{16})^2 + 16A_{13}(A_{15} - A_{18} + A_{23})$$

Similarly at $+\infty$ we use the transformation

$$(4.6) \qquad h = Y + 1 \quad , \quad \tilde{h} = \tilde{Y}$$

The Euler equations (2.8) assume the form

$$\begin{aligned} &-2AY'' - A_1\tilde{Y}'' + \tilde{Y}'[Y(2A_9 - A_5) + (A_{10} - 2A_7)\tilde{Y} + 2A_9 - A_5 - A_6] \\ &+ 4A_{13}Y^3 + 12A_{13}Y^2 + 8A_{13}Y + A_{22}\tilde{Y}^3 + (2A_{23} + A_{18})\tilde{Y}^2 \\ &- 2(A_{16} + A_{14})\tilde{Y} - 3A_{16}Y^2\tilde{Y} - 2(3A_{16} + A_{14})Y\tilde{Y} + 2A_{23}\tilde{Y}^2Y = 0 \end{aligned}$$

$$\begin{aligned} (4.7) \quad &-A_1Y'' - 2A_2\tilde{Y}'' - Y'[(2A_9 - A_5)Y + (A_{10} - 2A_7)\tilde{Y} + 2A_9 - A_5 - A_6] \\ &- A_{16}Y^3 - (3A_{16} + A_{14})Y^2 - 2(A_{16} + A_{14})Y + 4A_{20}\tilde{Y}^3 + 3(A_{19} + A_{22})\tilde{Y}^2 \\ &+ 2(A_{23} + A_{18} + A_{15})\tilde{Y} + 3A_{22}\tilde{Y}^2Y + 2(A_{18} + 2A_{23})Y\tilde{Y} + 2A_{23}Y^2\tilde{Y} = 0 \end{aligned}$$

We seek the asymptotic solution in the form

$$(4.8) \qquad Y = b_1 \exp(-2\alpha_2 X) \quad ; \quad \tilde{Y} = \tilde{b}_1 \exp(-2\tilde{\alpha}_2 X)$$

where $b_1, \tilde{b}_1, \alpha_2, \tilde{\alpha}_2$ are constants and we find that

$$(4.9) \qquad \alpha_2 = \tilde{\alpha}_2 = \frac{1}{2}\sqrt{\frac{-C_1 + \sqrt{C_1^2 - 4C_0C_2}}{2C_0}}$$

and where

$$\begin{aligned} C_0 &= 4AA_2 - A_1^2 \\ C_1 &= -4A(A_{15} + A_{18} + 2A_{23}) - 4A_1(A_{16} + A_{14}) + (2A_9 - A_5 - A_6)^2 - 16A_2A_{13} \\ C_2 &= -4(A_{14} + A_{16})^2 + 16A_{13}(A_{15} + A_{18} + A_{23}) \end{aligned} \qquad (4.10)$$

The parameters α_1 and α_2 are the relaxation parameters we are looking for. In the case of monatomic gas

$$(4.11) \qquad \alpha_1 = \alpha_2 = \sqrt{\frac{A_{12}}{A}} = \frac{2}{\Lambda}$$

which is directly related to Prandtl's shock wave thickness. For gas mixtures there is no symmetry of the shock wave and the last equality is not applicable.

The relaxation parameters α_1 and α_2 do not provide full information on the shock wave structure, however they are convenient tools for the description of shock waves in binary gas mixtures and play similar role (as seen from (4.11)) as Prandtl's shock wave thickness in the case of monatomic gases. Moreover, they provide some information concerning the asymmetry of the shock wave.

5. Numerical methods

The asymptotic behaviour of the solution of the Euler equations is taken into account in numerical procedures described below.

Let $\varphi(x)$ be an auxiliary monotonic smooth function with the following properties (App.B)

$$(5.1) \qquad \varphi(x) = \begin{cases} -1 & \text{at} \quad -\infty \\ +1 & \text{at} \quad +\infty \end{cases}$$

Thus

$$(5.2) \qquad \alpha(x) = \frac{\alpha_1 + \alpha_2}{2} - \frac{\alpha_1 - \alpha_2}{2}\varphi(x)$$

assumes the values of relaxation parameters at $\pm\infty$ and the functions

$$(5.3) \qquad \begin{aligned} h(x) &= y(x)\exp(-2\alpha(x)x\varphi(x)) + \operatorname{th}[\alpha(x)x], \\ \tilde{h}(x) &= \tilde{y}(x)\exp(-2\alpha(x)x\varphi(x)) \end{aligned}$$

have the required asymptotic behaviour. The functions y and $\tilde{y}$ describe the perturbation of the $th(\alpha(x))$ shock wave structure. They obey the following system of differential equations:

$$G_1 y'' + G_2 \tilde{y}'' + G_3 y' + G_4 \tilde{y}' + \sum_{j=0}^{3}\sum_{i=0}^{3} G_{ij}\, y^i \tilde{y}^j = 0$$

$$H_1 y'' + H_2 \tilde{y}'' + H_3 y' + H_4 \tilde{y}' + \sum_{j=0}^{3}\sum_{i=0}^{3} H_{ij}\, y^i \tilde{y}^j = 0 \qquad (5.4)$$

where functions G_i, H_i, G_{ij}, H_{ij} are specified in Appendix B.

This system of equation should be solved with the boundary conditions

$$y(\pm\infty) = \tilde{y}(\pm\infty) = 0 \qquad (5.5)$$

To solve numerically this two-point boundary value problem the iterative finite difference method has been applied [19]. For cross-checking of the numerical results two variants of the iterative method have been employed.

In the first one the following scheme was used

$$G_1 (1+\omega_r) y_j^{i+1} + G_2 (1+\omega_r) \tilde{y}_j^{i+1} = R_1^i$$

$$H_1 (1+\omega_r) y_j^{i+1} + H_2 (1+\omega_r) \tilde{y}_j^{i+1} = R_2^i \qquad (5.6)$$

where

$$R_1^i = G_1 \omega_r y_j^i + G_2 \omega_r \tilde{y}_j^i + G_1 [y_{j+1}^i + y_{j-1}^i]/2 + G_2 [\tilde{y}_{j+1}^i + \tilde{y}_{j-1}^i]/2 - K_1^i \Delta x^2/2.$$

$$R_2^i = H_1 \omega_r y_j^i + H_2 \omega_r \tilde{y}_j^i + H_1 [y_{j+1}^i + y_{j-1}^i]/2 + H_2 [\tilde{y}_{j+1}^i + \tilde{y}_{j-1}^i]/2 - K_2^i \Delta x^2/2.$$

$$K_1^i = -(G_3 y' + G_4 \tilde{y}' + \sum_{j=0}^{3}\sum_{i=0}^{3} G_{ij}\, y^i \tilde{y}^j)$$

$$K_2^i = -(H_3 y' + H_4 \tilde{y}' + \sum_{j=0}^{3}\sum_{i=0}^{3} H_{ij}\, y^i \tilde{y}^j)$$

and ω_r is over-relaxation parameter.

In the notation used above superscripts denote the iteration number whereas subscripts denote points in the net.
In the first step of the numerical solution of the system (5.6) we assume initial values y_j^0, $\tilde{y}_j^0$, for all $j, j=1,1...N$

Further at each step of iteration we solve the system of linear equations (5.6) with the boundary conditions

$$(5.7)\quad y_0^{i+1} = \tilde{y}_0^{i+1} = y_N^{i+1} = \tilde{y}_N^{i+1} = 0$$

The value of ω_r is selected to insure convergence of the iteration process [19-20] .
In the second approach, the so called matrix factorization method [24-22] , we use again the over-relaxation parameter ω_r but in this case the iteration scheme of solving (5.4) is defined by

$$\begin{aligned} &y_{j+1}^{i+1} - 2(1+\omega_r)y_j^{i+1} + y_{j-1}^{i+1} = R_1^i \\ (5.8)\quad &\tilde{y}_{j+1}^{i+1} - 2(1+\omega_r)\tilde{y}_j^{i+1} + \tilde{y}_{j-1}^{i+1} = R_2^i \end{aligned}$$

where

$$R_1^i = -2\omega_r y_j^i + \Delta x^2 (K_2^i - H_2 K_1^i/G_2)/(H_1 - H_2 G_1/G_2)$$

$$R_2^i = -2\omega_r \tilde{y}_j^i + \Delta x^2 \{K_1^i/G_2 - G_1[(K_2^i - H_2 K_1^i/G_2)/(H_1 - H_2 G_1/G_2)]/G_2\}$$

K_1^i, K_2^i being defined as above.
Equations (5.8) in the matrix representation can be written as

$$(5.9)\quad -A_j Y_{j+1}^{i+1} + B_j Y_j^{i+1} - C_j Y_{j-1}^{i+1} = F_j^i$$

where $Y_j^i = \begin{pmatrix} y_j^i \\ \tilde{y}_j^i \end{pmatrix}$, $F_j^i = \begin{pmatrix} R_1^i \\ R_2^i \end{pmatrix}$

$$A_j = \begin{bmatrix} -1 & 0 \\ 0 & -1 \end{bmatrix} , \quad B_j = \begin{bmatrix} -2(1+\omega_r) & 0 \\ 0 & -2(1+\omega_r) \end{bmatrix} , \quad C_j = A_j$$

The matrix factorization method can be now expressed by an iterative formula

$$(5.10)\quad Y_j^{i+1} = X_j^{i+1} Y_{j+1}^{i+1} + Z_j^{i+1}$$

where the matrix X_j^i is given by

$$(5.11)\quad X_j^{i+1} = (B_j - C_j X_{j-1}^{i+1})^{-1} A_j$$

and the vector Z_j^{i+1} by

$$(5.12)\quad Z_j^{i+1} = (B_j - C_j X_{j-1}^{i+1})^{-1} (F_j^i + C_j Z_{j-1}^{i+1})$$

The form of matrices A, B and C assure the stability of the matrix factorization process [19,23] .

6. Shock waves in monatomic one-component gases

The normal shock wave in one-component monatomic gas belongs to the most widely studied phenomena in gas dynamics [10-17,24-35] because it is the simplest flow in which large departures from equilibrium occur.

Since the non-equilibrium behaviour in a shock wave is directly related to the intermolecular collisions the shock structure depends on the intermolecular collision law. Therefore, the details of shock structure concerning the microscopic and macroscopic properties are of great physical interest and under the suitable conditions can provide some information on intermolecular potentials.

The shock wave phenomena were investigated within the framework of the kinetic theory [10-17],[24-35] as well as continuum theory [36-38]. The last one is satisfactory for weak shocks. Unfortunately, the kinetic approach is complicated by the approximation necessary to solve the Boltzmann equation. A broad review of these numerous theoretical methods and results is presented in survey papers by W.Fiszdon [39] and W.Fiszdon, R.Herczyński, Z.Walenta [40,41] . There are also several results connected with experimental investigation [42-52] .

In this paper we start with an analysis of the structure of shock waves in a one-component, monatomic gas for realistic Lennard-Jones potentials using for this purpose the Mott-Smith approach combined with the variational method.

The variational methods were discussed in some papers and also applied in shock wave structure calculations for rigid sphere molecules model [1, 15-16, 53-54].

The parameters characterizing the gas far in front of ($at -\infty$) and far behind ($at +\infty$) the shock wave are linked by the Rankine-Hugoniot conditions [36].

$$(6.1)\qquad n^+ = n^- \frac{(\gamma+1)(M^-)^2}{2+(\gamma-1)(M^-)^2} = n^- H_n(M^-)$$

$$(6.2)\qquad T^+ = T^- \frac{[2\gamma(M^-)^2-(\gamma-1)][(\gamma-1)(M^-)^2+2]}{(\gamma+1)^2(M^-)^2} = T^- H_T(M^-)$$

$$(6.3)\qquad v^+ = v^- \frac{2+(\gamma-1)(M^-)^2}{(\gamma+1)(M^-)^2} = v^- H_v(M^-)$$

where $M^- = \frac{v^-}{\sqrt{\gamma RT^-}}$ is the Mach numer in front of the shock wave and $\gamma = c_p/c_v$ is the isentropic index.

In terms of the parameters at $-\infty$ the solution of the one-dimensional Boltzmann equation for a shock wave and for a given Lennard-Jones (s_2-s_1) potential $\Phi(r) = 4\epsilon\left[\left(\frac{\sigma}{r}\right)^{s_1} - \left(\frac{\sigma}{r}\right)^{s_2}\right]$ is:

$$(6.4)\qquad f(\underline{c}, x; n^-, T^-, v^-; \epsilon, \sigma, m) = n^-\left(\frac{4kT^-}{m}\right)^{-3/2} \hat{f}(\hat{\underline{c}}, \hat{x}; \hat{n}^-, M^-; \hat{\epsilon})$$

where the non-dimensional parameters are dashed and are defined:

$$(6.5)\qquad \hat{x} = \frac{x}{\sigma}\,,\quad \hat{\underline{c}} = \sqrt{\frac{\mu}{2kT^-}}\,\underline{c}\,,\quad \hat{\underline{v}} = \sqrt{\frac{\mu}{2kT^-}}\,\underline{v}\,,\quad \hat{n} = n\sigma^3,\ \hat{\epsilon} = \frac{\epsilon}{kT^-}$$

and where:

k - is Boltzmann constant,

μ - is the reduced mass of colliding molecules

σ, ϵ-are parameters of the potential(force constants)

namely: ϵ is the depth of the potential well; σ is the collision diameter for low energy collisions (the value of r for which $\Phi(r) = 0$.)

The Prandtl shock wave thickness is:

$$(6.6) \qquad \Lambda = \frac{n^+ - n^-}{\left(\frac{dn}{dx}\right)_{max}}$$

From (6.4) and (6.5) on the basis of dimensional analysis we obtain:

$$(6.7) \qquad \left(\frac{dn}{dx}\right)_{max} = (n^-)^2 \sigma^2 \hat{F}(\hat{n}^-, M^-, \hat{\epsilon})$$

and hence

$$(6.8) \qquad \Lambda = \frac{H_n(M^-) - 1}{n^- \sigma^2 \hat{F}(\hat{n}^-, M^-, \hat{\epsilon})} = \frac{\sigma (H_n(M^-) - 1)}{\hat{n}^- \hat{F}(\hat{n}^-, M^-, \hat{\epsilon})}$$

The mean free path at $-\infty$ is [55-56]

$$(6.9) \qquad \lambda^- = \left[\sqrt{2}\,\pi\, n^- \sigma^2 \Omega^{(2,2)*}(\hat{\epsilon}^{-1}, s_1, s_2)\right]^{-1}$$

where $\Omega^{(2,2)*}$ is tabulated in [18]. Hence, the non-dimensional shock wave thickness

$$(6.10) \qquad \frac{\Lambda}{\lambda^-} = \frac{\sqrt{2}\,\pi\, \Omega^{(2,2)*} [H_n(M^-) - 1]}{\hat{F}(\hat{n}^-, M^-, \hat{\epsilon})}$$

depends on $\hat{n}^-, M^-$ and $\hat{\epsilon}$.

The values of λ^-/Λ obtained from experiments in shock tubes for a given Mach number are not far apart in spite of the fact that different gases were used and that the initial conditions in different experiments were not the same. This fact suggests that there is a universal relation between λ^-/Λ and the Mach number M^-, valid for all gases and all experimental conditions and in a number of papers [41,58] this hypothesis has been tacitly assumed.

From (6.10) it follows that there is no theoretical basis for such hypothesis but the proximity of experimental points demands theoretical explanation.

The first result in this direction belongs to Muckenfuss [11] who showed that for point centers of repulsion potential (purely repulsive potential) $\phi \sim r^{-s}$, λ^-/Λ depends only on Mach number, M^- (and s). Muckenfuss used the Mott-Smith distribution function and he applied the moment method with an additional moment equation for c_x^2.

We will show that the same result follows from our analysis and that in the case of a Lennard-Jones potential λ^-/Λ, as a function of M^-, depends on the parameter $\hat{\epsilon}$.

From our previous consideration it follows that this result is valid if the function $\hat{F}$ in (6.7) is independent of $\hat{n}$.

Introducing non-dimensional variables (6.5) we can write

$$(6.11)\qquad f^-(\underline{c}) = n^-\left(\frac{2\pi kT^-}{m}\right)^{-3/2} \exp\left\{-\frac{(\underline{c}-\underline{v}^-)^2}{\frac{2kT^-}{m}}\right\} = n^-\left(\frac{4kT^-}{m}\right)^{-3/2} \hat{f}^-(\hat{\underline{c}})$$

where

$$(6.12)\qquad \hat{f}^-(\underline{c}) = \left(\frac{\pi}{2}\right)^{-3/2} \exp\left[-2(\hat{\underline{c}}-\hat{\underline{v}}^-)^2\right]$$

and using (6.1) - (6.3)

$$(6.13)\qquad f^+(\underline{c}) = n^+\left(\frac{2\pi kT^+}{m}\right)^{-3/2} \exp\left\{-\frac{(\underline{c}-\underline{v}^+)^2}{\frac{2kT^+}{m}}\right\} = n^-\left(\frac{4kT^-}{m}\right)^{-3/2} \hat{f}^+(\hat{\underline{c}}),$$

where

$$(6.14)\quad \hat{f}^{+}(\hat{\underline{c}}) = \left(\frac{\pi}{2}\right)^{-3/2} H_{\infty}(M^{-})\left[H_{T}(M^{-})\right]^{-3/2} \exp\left\{-\frac{2(\hat{c}-\hat{v}^{-}H_{v}(M^{-}))^{2}}{H_{T}(M^{-})}\right\}$$

As $\hat{v}^{-} = \sqrt{T}M^{-}/2$ both $\hat{f}^{-}$ and $\hat{f}^{+}$ depend only on M^{-}.
From (2.13) it follows that

$$(6.15)\quad \Lambda = 2\sqrt{\frac{A}{C}} = \frac{2\sigma}{\hat{n}^{-}}\sqrt{\frac{\hat{A}}{\hat{C}}}$$

where $\hat{A}$ and $\hat{C}$ are obtained from formulae for A and C (App.A) by replacing f^{-} and f^{+} by $\hat{f}^{-}$ and $\hat{f}^{+}$.
From the formulae (App.A) it follows that $\hat{A}$ depends only on M^{-} whereas $\hat{C}$ depends both on M^{-} and on the intermolecular potential.
In terms of non-dimensional variables the collision dynamics described by (3.5) remains valid if we replace $\underline{c}, \underline{c}_{*}, \underline{c}', \underline{c}'_{*}$, g by dashed magnitudes $\hat{\underline{c}}, \hat{\underline{c}}_{*}, \hat{\underline{c}}', \hat{\underline{c}}'_{*}, \hat{g}$ $\left(\hat{g} = g\sqrt{\frac{m}{2kT}}\right)$.
The intermolecular potential enters the collision dynamics only through the impact angle Ψ (cf. 3.2) which now can be written in the form[18]:

$$(6.16)\quad \Psi(\hat{b},\hat{g}) = \int_{-\infty}^{\hat{r}_{min}} \frac{\hat{b}\,d\hat{r}}{\hat{r}^{2}\left[1-\left(\frac{\hat{b}}{\hat{r}}\right)^{2}-\frac{\hat{\Phi}(\hat{r})}{\hat{g}^{2}}\right]^{1/2}}; \quad \hat{\Phi}(\hat{r}) = \frac{\Phi(r)}{kT}, \quad \hat{b} = \frac{b}{\sigma}$$

For the Lennard-Jones - (s_2, s_4) potential

$$(6.17)\quad \hat{\Phi}(\hat{r}) = 4\hat{\epsilon}\left[(\hat{r})^{-s_4} - (\hat{r})^{-s_2}\right]$$

the velocities of colliding molecules after the collision $\hat{\underline{c}}', \hat{\underline{c}}'_{*}$, depend only on $\hat{\epsilon}$, $\hat{b}$ and $\hat{\epsilon}$ and on the velocities of those molecules before the collision, $\hat{\underline{c}}, \hat{\underline{c}}_{*}$.
Thus performing the integration over $\hat{b}, \hat{\epsilon}, \hat{\epsilon}$ and $\hat{\underline{c}}_{*}$ we get

$$(6.18)\quad \hat{C} = \hat{C}(M^{-}, \hat{\epsilon})$$

and from (6.15) it follows that

$$(6.19)\quad \Lambda = \frac{2\sigma}{\hat{n}^-}\hat{G}(M^-,\hat{\epsilon}) \quad , \quad \hat{G}(M^-,\hat{\epsilon}) = \sqrt{\frac{\hat{A}(M^-)}{\hat{C}(M^-,\hat{\epsilon})}}$$

and $\frac{\Lambda}{\lambda^-}$ is independent of $\hat{n}^-$ ((6.19), (6.9)) .

Note that in the considered approach the function $\hat{f}$ in (6.4) depends on $\hat{n}^-$.

From (2.9) we get

$$(6.20)\quad \hat{f}(\hat{x},\hat{\underline{c}}) = \frac{1-\hat{h}(\hat{x})}{2}\hat{f}^-(\hat{\underline{c}}) + \frac{1+\hat{h}(\hat{x})}{2}\hat{f}^+(\hat{\underline{c}})$$

and

$$(6.21)\quad \hat{h}(\hat{x}) = \mathrm{th}\frac{2\hat{x}}{\hat{\Lambda}} = \mathrm{th}\left(\frac{\hat{x}\hat{n}^-}{\hat{G}(M^-,\hat{\epsilon})}\right)$$

where

$$(6.22)\quad \hat{h}(\hat{x}) = \hat{h}(\hat{x};\hat{n}^-,M^-,\hat{\epsilon}) \quad , \hat{\Lambda} = \frac{\Lambda}{\sigma} \; ; \; \hat{f}^{\pm}(\hat{\underline{c}}) = \hat{f}^{\pm}(\hat{\underline{c}};M^-)$$

For the point centers of repulsion potential in the form

$$(6.23)\quad \Phi = \tilde{\epsilon}\left(\frac{\sigma}{r}\right)^s$$

we can replace σ in (6.5) by $\tilde{\sigma} = \sigma\left(\frac{\tilde{\epsilon}}{kT^-}\right)^{1/s}$ which leads to

$$(6.24)\quad \Lambda = \frac{2}{\tilde{\sigma}^2 n^-}\sqrt{\frac{\hat{A}}{\hat{C}}} = \frac{2\sigma}{\hat{n}^-}\left(\frac{kT^-}{\tilde{\epsilon}}\right)^{2/s}\sqrt{\frac{\hat{A}}{\hat{C}}}$$

but with $\hat{C} = \hat{C}(M^-)$. In this case [55-56]

$$(6.25)\quad \lambda^- = \left[\sqrt{2}\,\pi n^-\sigma^2 \tfrac{1}{2}\tilde{A}_2(s)\,\Gamma\left(4-\tfrac{2}{s}\right)\left(\frac{s\tilde{\epsilon}}{kT^-}\right)^{2/s}\right]^{-1}$$

where $\tilde{A}_2$ is a tabulated function [18,55]. Hence λ/λ^* depends only on M^- (and on the repulsion exponent s). This conclusion coincides with that of Muckenfuss mentioned before.

In Fig.2 the dependence of λ^-/λ on Mach number M^- is presented both for the Lennard-Jones (6-12) potential and for the purely repulsive potential, $\phi \sim r^{-12}$. The former one depends on $\hat{\epsilon}$ and it is seen that for a given M^- the non-dimensional shock wave thickness increases with the rise of $\hat{\epsilon}$. All curves and also a curve for purely repulsive potential practically coincide for M^- up to about 1.6. For high Mach numbers the curves obtained for the Lennard-Jones potential are almost parallel.

The curve for the purely repulsive potential does not belong to the family of curves for the Lennard-Jones potential and cannot be treated as the limiting case for $\hat{\epsilon} \to 0$.

The comparison of our results for purely repulsive potential with some theoretical results is given in Fig.3. Although the overall shape of presented curves for different s remains unaltered the numerical values differ considerably in particular for high Mach numbers.

The comparison of theoretical results (Lennard-Jones potential) with the experimental data is presented in Fig's: 4 (argon) and 5 (helium). The value of $\epsilon/k = 116^\circ K$ for argon was obtained [18] via viscosity measurements in the temperature range 300-1000°K.

Experiments as well as our calculations were performed for $T^- = 300^\circ K$ which gives $\hat{\epsilon} = 0.387$. The agreement between the presented theory and experimental data seems to be satisfactory, better than for purely repulsive potential which predicts higher values of λ^-/λ for Mach numbers M^- between 2 and 3.

For helium (Fig.5) we took $\epsilon/k = 10.22^\circ K$, the value obtained from the viscosity data for 80-300°K, i.e. for temperatures much lower than those in presented experiments with shock waves, where $\hat{\epsilon} = 0.034$. Perhaps, this explains the discrepancy of experimental results and our theory.

The experimental values of λ^-/λ agree much better with theoretical values obtained for the Lennard-Jones (6-9) potential

and for $\hat{\epsilon}$ =0.034 (which corresponds to $\frac{\epsilon}{k}$ =10.22°K) than with values obtained for the Lennard-Jones (6-12) potential and for $\hat{\epsilon}$ = 0.034.

It is clear that due to the relatively large scatter of experimental data as well as the uncertainity of the values of ϵ/k entering the Lennard-Jones potential no final conclusion from the above comparisons can be drawn.

Our results confirm the fact that experimental points obtained in shock tube experiments for a given Mach number but for different gases are close to each other; in all these experiments T^- = 300°K and hence the values of $\hat{\epsilon}$ for different gases are in a relatively narrow range. For this range of $\hat{\epsilon}$ theoretical curves are not far apart.

The situation changes if the experiments are performed in wind tunnels. In this case T^- is of order of a few °K and the values of $\hat{\epsilon}$ are usually very high.

For example in the experiment of T.Holtz [51] , made for the shock wave in argon, T^- = 16°K and hence $\hat{\epsilon}$ = 7.25.

This experiment was perform for M^- =7.18 and the value λ^-/Λ = 0.12 was obtained.Taking the Lennard-Jones(6-12) potential and $\hat{\epsilon}$=7.25 from our theory we get λ^-/Λ = 0.18.

However, the results concerning the parallel and perpendicular velocity distribution functions $f_\parallel, f_\perp$ suggest a good agreement between our results obtained for the Lennard-Jones (6-12)potential and experimental data. (Fig.6).

The both profiles (for parallel and perpendicular velocity distribution functions) are only slightly narrower than experimental profiles.

In the case of one-component gas the shock wave thickness, Λ , fully characterizes the shock wave structure in monatomic gases. But for some experiments it is convenient to compare directly the obtained shock wave structure with that obtained theoretically.

In terms of the reduced parameters $\bar{n}, \bar{T}, \bar{v}$:

$$(6.26)\quad \bar{n}(x)=\frac{n(x)-n^-}{n^+-n^-}\quad,\quad \bar{T}(x)=\frac{T(x)-T^-}{T^+-T^-}\quad,\quad \bar{v}=\frac{v(x)-v^+}{v^--v^+}$$

the shock wave profiles are:

$$\bar{n}(x) = \frac{1 + h(x)}{2} \tag{6.27}$$

$$\bar{T}(x) = \frac{n^+(1 + h(x))}{(n^+ + n^-) + h(x)(n^+ - n^-)} \tag{6.28}$$

$$\bar{V}(x) = \frac{n^-(1 - h(x))}{(n^+ + n^-) + h(x)(n^+ - n^-)} \tag{6.29}$$

All these profiles have the same Prandtl's shock wave thickness.

$$\frac{1}{2} - \bar{n}(-x) = -\frac{1}{2} + \bar{n}(x) \tag{6.30}$$

$$\frac{1}{2} - \bar{T}(d - x_*) = -\frac{1}{2} + \bar{T}(d + x_*) \tag{6.31}$$

$$\frac{1}{2} - \bar{V}(d - x_*) = -\frac{1}{2} + \bar{V}(d + x_*) \tag{6.32}$$

where: $x_* = x - d$ and

$$d = -\frac{\Lambda}{2} \operatorname{Arth} \frac{n^+ - n^-}{n^+ + n^-} = -\frac{\Lambda}{2} \operatorname{Arth} \frac{(M^-)^2 - 1}{\frac{5}{3}(M^-)^2 + 1} \tag{6.33}$$

The centers of temperature and velocity shock wave profiles coincide and, as it is seen from the above formulae, they are shifted upstream with respect to the center of the density profile. The shock wave structure in monoatomic gas is shown in Fig.7.

Finally it is of some interest to look at the changes of the distribution function along the x-axis. In Fig.8 we show the velocity distribution function within the shock wave for argon,

$M^{-} = 2.5$ and for the Lennard-Jones(6-12) potential.

7. Binary gas mixtures.

The shock wave structure in binary gas mixture have been studied first in several theoretical [59-64] and later in both experimental [65-68] and theoretical papers [69].

The continuum theory approach was applied by Cowling [59], Dyakov [60] , Sherman [62] , Goldman and Sirovich [69] . This problem was also discussed by Zeldovich and Raizer [36]. All analyses predict separation of gases within the shock wave which leads to a marked broadening of the shock wave.

It was quickly realized, that a fuller investigation of strong shock waves should be done in the framework of the kinetic theory.

The Mott-Smith approach was widely applied to the investigation of the shock wave structure in gas mixtures. The first attempt by Fujimoto [70] was unsuccessful because the assumptions concerning the form of distribution functions were unrealistic and therefore conservation of momentum and energy within the shock wave was not fulfilled. Tanenbaum and Scott [71] concluded that the mixture problem cannot be solved using the Mott-Smith bimodal description.

It was pointed out [71] ,that even in cases of multimodal distribution functions in which the velocities and temperatures associated with Maxwellians are constant, there appear artificial restrictions predetermining separation. Therefore, a multimodal description does not give physically acceptable results. This difficulty was overcome by M.M.Oberai [72] and M.M.Oberai and U.N.Singha [73] . They postulated distribution functions as generalized Mott-Smith distribution functions for both components. The temperature and velocity appearing in a certain Maxwellian form [73] depend on the position within the shock waves. M.M.Oberai and U.N.Singha applied the moment method considering Maxwellian molecules and rigid sphere molecules.

The purely numerical approach by means of the Monte Carlo method was used by Bird [74] to investigate argon-helium mixtures.

M.Sinclair and J.M.de Leeuw [75] combined the moment method and Mott-Smith approach (applied only to the light gas component) with the Monte Carlo method related only to the heavy gas species. The heavy particle flow pattern induced by the light gas shock wave was built up using a test particle Monte Carlo approach. Also in this work rigid spheres and Maxwellian molecules models were used.

Experimental research of shock wave structure in mixtures was performed in the sixties by Center [66] , Harnett,Muntz [76] Rothe [88], Beylich [68]. Later interesting results were obtained by A.Gmurczyk, Z.Walenta and M.Tarczyński [1-2]. They indicated the characteristic "hump" at the density distribution for the light component within the shock wave (in helium-xenon mixture). This phenomenon was observed for binary mixtures of gases with disparate masses and for a small mole fraction of the heavy component,xenon.

The BGK method was widely used in sixties for the investigation of the shock wave structures in binary gas mixtures [77-81] . W.Piszdon and T.Płatkowski considered structures of shock waves in diatomic gases and in mixtures of noble and diatomic gases with comparable atomic masses using BGK approach [77].The BGK method was also applied in Płatkowski's works [78-81] where the author investigated the shock wave structures in a binary gas mixture of noble and diatomic gases. However,it should be noticed that the methods used in the above papers do not give the possibility to take into account directly the proper physical intermolecular potential.

Recently P.Mausbach investigated [82- 83] the shock wave structure in the binary gas mixture considering the rigid spheres model and using iterative method to solve Boltzmann equations. This method was an extension of the method developed by Tcheremissine [84] and the method of operator splitting proposed by Tcheremissine and Aristov [85] .

As mentioned in the introduction ,our paper presents some results concerning shock wave structures in binary gas mixture for more realistic intermolecular potential.
The present results generalize our previous ones [8-9] concerning shock wave structures in gas mixtures of helium and xenon molecules represented by rigid elastic spheres with

different diameters. Here the Lennard-Jones (6-12) intermolecular potential was used for two gas mixtures, namely helium-xenon and helium-argon.

For these mixtures the results of experiments performed by A.Gmurczyk, M.Tarczyński and Z.Walenta [1,2] were available. It should be noted that the above-mentioned experiments will be repeated because of relatively low accuracy of available experimental results [private communication of Z.Walenta]. The principal difference between the description of the shock wave structure in a one-component gas and in a gas mixture is in the role of the shock wave thickness Λ. The Prandtl's shock wave thickness Λ fully determines the shock wave structure in the one-component gas, whereas the relaxation parameters α_1, α_2 introduced (section 4) instead of Λ do not describe uniquely the shock wave structure in a gas mixture. There is also no analytical solution comparable to the solution (2.12). However, it is possible to show, similarly as in the case of one-component gas (section 6), that the dimensionless shock wave thickness (in Prandtl's definition or defined through relaxation parameters (e.g. $\frac{\Lambda^*}{\lambda^*} = \frac{4}{(\alpha_1+\alpha_2)\lambda^*}$) and also $\alpha_1\lambda^*$, $\alpha_2\lambda^*$) obtained in the presented approach are independent of $\hat{n}^*$; (where $\hat{n}^* = n^*\sigma_{12}^3$ -(see Appendix C), σ_{12} is here potential parameter for the interaction between unlike molecules). As mentioned in the introduction to this paper some results concerning shock wave structures in a binary gas mixture for more realistic intermolecular potential are preseted.

Figures 9-21 show results concerning two binary gas mixtures of nonreacting gases with disparate molecular masses: helium-xenon and helium-argon. They present the average velocity, number density and temperature distributions for both components within the shock wave. In all cases the velocity, density and temperature separation between both species is observed.

Figures 9-11 relate to the xenon-helium mixture with mole fraction of xenon: $w_{Xe} = n_{Xe}^*/(n_{Xe}^*+n_{He}^*) = 0.06$. The mass concentration of xenon is: $C_{Xe} = w_{Xe}\beta/(1+w_{Xe}(\beta-1))$, where $\beta = \frac{m_{Xe}}{m_{He}}$ and in this case: $C_{Xe} = 0.893$.

The number density profile for the lighter gas component has a characteristic "hump" for the cases: $M^* = 1.5$ and 2.5

whereas the number density distribution for the heavy gas component(xenon)is monotonic. It is also shown that with the rise of $\bar{M}$ this "hump" disappears . In all cases there is a considerable "overshoot" of the temperature of the heavy component,xenon. Xenon temperature overshoots the downstream equilibrium value within the shock wave as collisions randomize the energy associated with the diffusion velocity between the two species.

The overshoot of the reduced temperature $\bar{T}$ is most marked in the case of the weak shock wave, $\bar{M} = 1.5$. However, the overshoot of the dimensionless temperature T/T^{-} is the highest one for the strong shock wave, $\bar{M} = 4.4$.

The distribution of the helium temperature is monotonic for $\bar{M} = 2.5$ and $\bar{M} = 4.4$ but it has a characteristic minimum within the shock wave for $\bar{M} = 1.5$ (Fig.9 b,c). The minimum appears also for the helium velocity profile in the case of $\bar{M} = 1.5$ (Fig. 9 a).

These results suggest the following physical explanation of the observed phenomena. In the mixture of gases with disparate masses, say helium-xenon , with the equal mole fractions of both components, the light component is compressed first because the frequency of helium-helium collisions is much higher than the frequency of xenon-xenon collisions. This effect is obviously enhanced when the mole fraction of xenon in the helium -xenon mixture is small. The compression of xenon follows that of helium and is due mainly to helium-xenon collisions. This time-lag between the formation of the shock wave in helium and in xenon leads to spatial separation of the shock wave structures for both components.The compression of the xenon component is accompanied by the rapid rise of xenon temperature due to the energy transfer resulting from helium-xenon collisions which randomize the energy associated with the diffusion velocity between the two species. Thus the rise of the xenon temperature is linked with the transfer of kinetic energy of the translational motion from helium to the xenon component and with the reduction of the internal energy of helium. This leads to the overshoot of the xenon temperature. It is

interesting to note that in the case of the Mach number $M = 1.5$ it was observed that the kinetic energy of translational motion of helium reaches a minimum within the shock wave and this corresponds to the maximum of the xenon temperature.

At the tail of the shock wave the process of equilibration takes place and velocities, densities and temperatures of both components reach their equilibrium values.

The next figures (12-14) are related to shock waves: $M = 1.6$ in the binary gas mixtures argon-helium with different argon mole fraction $W_{Ar} = 0.05, 0.3, 0.5$, respectively: with mass concentration of argon $C_{Ar} = 0.344, 0.810, 0.909$. First, we noticed that the separation between number densities for both components rises with the rise of mole fraction of the heavy component. The separation (for considered cases) is the most significant for $W_{Ar} = 0.5$, however it does not relate to the maximum shock wave thickness (Prandtl's definition - for the case of gas mixture). The overshoot of argon temperature appears only for small mole fraction of argon. For larger W_{Ar} the monotonic character of temperature profiles is observed. The effect of the temperature overshoot for the helium-argon mixture has been already predicted in many papers [74, 75, 83, 86]. It is also interesting to see how the shock wave thickness in Prandtl's version changes with W_{Ar}. Fig. 15 shows the comparison of the experimental data obtained by Center [66] with a theory by Goldmann and Sirovich [69]. Our results fit quite well the experimental data; however, they are even in better agreement with theoretical results obtained by Goldmann and Sirovich [69]. The maximum of the shock wave thickness appears for a higher value of mole fraction W_{Ar} than in Center's experiments.

It was discussed in section 4 that the maximum-slope thickness (Prandtl's definition) is a poor characteristic of the profile shape since it depends on a purely local property of the shock wave. The shock wave description can be, however, improved by adding the relaxation coefficients α_1, α_2 related to the process of equilibration at $\pm\infty$. From these coefficients we can form "modified" shock wave thickness Λ^*:

(7.1) $$\Lambda^* = \frac{4}{\alpha_1 + \alpha_2}$$

which also is incomplete characteristic of the shock wave and we can introduce also the asymmetry coefficient $a_s = \alpha_2/\alpha_1$.

Fig.16 shows the dependence of a_s on w_{Ar} for a helium-argon mixture. The most significant asymmetry (Fig.16) appears for the shock wave with a small argon mole fraction.

Fig.17 presents the change of λ^-/Λ^* and $\alpha_1\lambda^-/2$, $\alpha_2\lambda^-/2$ with Mach number M^- for a xenon-helium mixture.

It should be noticed that although the theoretical approach prefers the use of α_1, α_2 it is not easy to extract these values from experiments because as a rule the experimental data obtained for the "tails" of the shock wave structure are much less accurate than those from the middle of the shock wave.

Figures 18-19 show velocity distribution functions within the shock wave structure for the mixture xenon-helium: $M^- = 4.4$, $w_{Xe} = 0.06$. The velocity distribution function of the light component has a bimodal character in the centre of the shock wave. This bimodal character does not exist in the case of the distribution function of the heavy component (Fig.19).

It is clear that the functional (2.4) characterizes also the accuracy of the method in the global approach. It is convenient to define the relative global error for the shock wave structure in a binary gas mixture as:

(7.2) $$\delta_{glob} = \frac{\int\left\{\int\left[\underline{\xi}\,\mathrm{grad}\, f_1 - \chi_1\right]^2 d^3\underline{c} + \int\left[\underline{\xi}\,\mathrm{grad}\, f_2 - \chi_2\right]^2 d^3\underline{c}\right\} dx}{2\int\left\{\int\left[\chi_1(f_1,f_2)\right]^2 d^3\underline{c} + \int\left[\chi_2(f_1,f_2)\right]^2 d^3\underline{c}\right\} dx} =$$

$$= \frac{\int S_{lok}\, dx}{2\int\left\{\int\left[\chi_1(f_1,f_2)\right]^2 d^3\underline{c} + \int\left[\chi_2(f_1,f_2)\right]^2 d^3\underline{c}\right\} dx}$$

where: $\chi_1 = \chi_{11} + \chi_{12}$, $\chi_2 = \chi_{21} + \chi_{22}$

Similarly, the relative maximum local error (in the centre of the shock wave structure) will be defined:

(7.3) $$\delta_{lok} = \frac{S_{lok}(0)}{2\left\{\int\left[\chi_1(f_1,f_2)\right]^2 d^3\underline{c} + \int\left[\chi_2(f_1,f_2)\right]^2 d^3\underline{c}\right\}}$$

It should be however noticed that in the method discussed here the global error is minimized.

Fig.s 20 a,b show the dependence of the global error and the maximum local error on the Mach number, $\bar{M}$. These results indicate that the best accuracy is reached for Mach numbers 2.5÷ 5. Unfortunately, for very high Mach numbers this accuracy decreases again due probably to a poor determination of the coefficients ((2.7) , Appendix A) by means of the Monte Carlo procedure.

The comparison of our results with experimental ones by A.Gmurczyk,M.Tarczyński,Z.Walenta as well as with theoretical results by Płatkowski [80](Fig.21) and Mausbach [83] indicate that the obtained number density separation is much smaller than that obtained by other authors. The overshoot of temperature for heavy component is more significant in our model and there is a qualitative agreement with the recent results obtained by Mausbach for helium - argon mixture.

To summarize results we can formulate the following conclusions

1. The heavy gas component temperature overshoots its downstream equilibrium value in the case of a mixture of gases with disparate molecular masses and for a small mole fraction of the heavy component. Also,in this case the characteristic "hump" appears on the lighter component density curve within the shock wave.

2. The "overshoot" of the dimensionless temperature T/T^- increases with the Mach number in front of the shock wave,$\bar{M}$.

3. The distribution function of the light component has a strong bimodal character, which especially is marked in the centre of the shock wave.
   This bimodal character does not appear for the velocity distribution function of the heavy component.

4. The Mott- Smith idea combined with Tamm's variational approach seems to be an efficient method,from the point of view of numerical calculations,and especially useful for the investigation of moderately strong shock waves $\bar{M} \sim 2 \div 6$ (Fig. 20). This method may be also applied

to the determination of intermolecular potentials.
In this case however, the high accuracy of calculation of the multiple integrals, entering as coefficients into Eulers equations (2.8), is needed. Experimental data of higher accuracy as those available at present for mixtures would be welcome to enable a good comparison with theoretical results.

Acknowledgement
The authors would like to express their deep appreciation and thanks to Prof.W.Fiszdon for his constant interest and for many suggestions and comments during the whole progress of this work and to Dr Z.Walenta for his valuable contribution.

References

1 A.S.GMURCZYK, M.TARCZYŃSKI, Z.A.WALENTA - Struktura fali uderzeniowej w mieszaninie gazów szlachetnych, IPPT report, 60 , Warszawa, 1978 .

2 A.S.GMURCZYK, M.TARCZYŃSKI, Z.A.WALENTA, XI RGD , 1979, p.333.

3 E.A.JOHNSON, Phys. of Fluids 21, 1239 , 1978

4 R.J.HUCK, E.A.JOHNSON, XII Symposium on Advanced Problems and Methods in Fluid Mech., Błażejewko 1979.

5 I.E.TAMM, Trudy Fiz. Inst. im. P.N.Lebiedeva, 29, 1965 , 239-249

6 M.N.KOGAN, Dinamika rozreshennovo gaza, Moskva , 1967

7 G.F.TAYLOR, Collected Papers, Cambridge, Univ. Press, 1963

8 M.BRATOS, R.HERCZYŃSKI, AMS, 32, 2 ,201, 1980

9 M.BRATOS, R.HERCZYŃSKI, Bulletin de l'Académie Pol. des Sciences, Serie des sciences techniques, v.XXVIII, No 5-6, 9, 1980 .

10 H.M.MOTT-SMITH, Phys. Rev. 82, 885 , 1951

11 CH.MUCKENFUSS, Phys. of Fluids, 5, 11, 1325 , 1962

12 V.QUAN, Phys. of Fluids, 10, 4, 889, 1967

13 P.D.LOHN, T.S.LUNDGREN, Phys. of Fluids, 17, 10, 1808, 1974

14 A.SAKURAI, J.Fluid Mech. 3, 255 , 1957

15. M.M.OBERAI, J.Mec. 6, 317 , 1967

16 R.NARASIMHA, S.M.DESHPANDE, J.Fluid Mech. 36, 555, 1969

17 R.NARASIMHA, VI RGD Nat. Bull. De la Classe des Sciences Ac. Roy Belge 5 Serie TLVI , 1970

18 JOSEPH O.HIRSCHFELDER, CH.F.CURTISS, R.B.BIRD, Molecular theory of gases and liquids, John Wiley & Sons, New York, London , 1964

19 E.ISAACSON, H.B.KELLER, Analysis of Numerical Methods, John Wiley & Sons, Inc. New York, London, Sydney, 1966

20 I.FRIED, Numerical solution of differential equation Academic Press, New York, San Francisco, London , 1979

21 R.D.RICHTMYER , K.W.MORTON, Difference methods for initial - value problems, Interscience Publ. John Wiley & Sons, 1967

22 N.N.JANENKO - Metod drobnych shagov rešenija mnogomernych zadač matematičeskoj fizyki - Izd.Nauka, Sybirskije Oddelenie, Novosibirsk ,1967

23 G.K.GODUNOV, V.S.PEBENSKIJ - Vvedenije v teoriju raznostnyh shem, Moskwa , 1962

24 G.A.BIRD, J.Fluid Mech. 30, 479 , 1967

25 H.W.LIEPMANN, R.NARASIMHA, & M.T.CHAHINE , Phys. of Fluids 5, 1313, 1962

26 R.NARASIMHA, Phys. of Fluids 9, , 2524 , 1966

27 R.NARASIMHA, J.Fluid Mech. 34, 1 , 1968

28 A.NORDSIECK , B.L.HICKS, Proceedings of the 5th International Symposium on Rarefied Gas Dynamics, Oxford 1, 695 , 1967

29 SHEE-MANG YEN, Winnie Ng, J.Fluid Mech., 65, p.1, 127, 1974

30 G.A.BIRD, Phys. of Fluids, 13, 5, 1172 , 1970

31 S.M.YEN, W.P.WALTERS, W.Ng, J.R.Flood, RGD, VIII, 1973

32 L.H.HOLWAY, Phys of Fluids, 9, 1658 , 1966

33 B.L.HICKS, S.M.YEN, RGD, Acad. Press., vol.I, 313 , 1969

34 B.L.HICKS, S.M.YEN, Phys. of Fluids 10, 458 , 1967

35 H.SALVEN, CH.E.GROSCH, S.ZIERING, Phys. of Fluids, 7, 180 , 1964

36 J.W.ZELDOVICH, J.R.RAIZER, Fizika udarnych voln, Nauka , 1966

37 D.GILBARG, D.PAOLUCCI, J.Rat.Mech. Anal., 2, 617, 1953

38 H.GRAD, Comm. Pure and Appl. Math . 2 , 336 , 1949 ; 5, 257 , 1952

39 W.FISZDON, Struktura płaskich fal uderzeniowych w jednoatomowych gazach, IPPT raport, 15/1978.

40 W.FISZDON, R.HERCZYŃSKI, Z.WALENTA, Engineering Transactions 24, 3, 629, 1976.

41 W.FISZDON, R.HERCZYŃSKI, Z.WALENTA, RGD, Proceedings of Ninth International Symposium (1974) p.Ax-B 23-1 v.II

42 B.SCHMIDT, J.Fluid Mech, 39, 361, 1969

43 H.ALSMEYER, Messung der Structur von Verdichtungsstösen in Argon und Stickstoff, Ph.D.Thesis, Universität Karlsruhe, 1974

44 M.LINZER "The structure of shock fronts in argon and nitrogen, Doctoral dissertation, Princeton University, Princeton 1961.

45 M.CAMAC, RGD ed. J.H.de LEEUW, Acad. Press. vol.1, 240, 1965

46 D.RUSSEL, RGD v.1, 265, Acad. Press., New York, 1965

47 F.SCHULTZ-GRUNOV, A.FROHN, RGD v.1, 250, Acad. Press, 1965

48 E.RIEUTORD, Doctoral Thesis, Lyon, 1970

49 M.LINZER, D.F.HORNIG, Phys. of Fluids 6, 1661, 1963

50 R.E.DUFF, W.M.WEBSTER, Bull. Am. Phys. Soc. 4, 283, 1959

51 T.HOLTZ Measurements of molecular velocity distribution functions in an argon normal shock wave at Mach number 7. Doctoral Dissertation, 1974.

52 B.T.BARCELO Electron beam measurements of the shock wave structure, Doctoral Dissert. 1971

53 P.ROSEN, The Journal of Chem. Physics, 22, 6, 1045, 1954

54 T.FUJITA, T.KODA, Y.WATANABE, Journal of the Physical Society of Japan; 32, 1, 67, 1972

55 S.CHAPMAN, T.G.COWLING, The mathematical theory of non-uniform gases, Cambridge, University Press, 1952.

56 CH.MUCKENFUSS, Phys. of Fluids, 5, 2, 1962

57 J.K.HAVILAND, Methods in Computational Physics, Advances in Research and Applications, v.4, New York, 109, 1965

58 C.CERGIGNANI, Theory and application of the Boltzmann equation, Scottish Acad. Press, 1975.

59 T.G.COWLING, Phil.Mag. 33, 61, 1942

60 S.P.DYAKOV, Zhur.Exp. Theor. Fiz. 27, 728, 1954

61 M.KOHLER, Zeit.f.Phys. 127, 40, 1949

62 F.S.SHERMAN, J.Fluid Mech., 8, 465, 1960

63 M.M.OBERAI, Phys. of Fluids, 8, 826, 1965

64 M.M.OBERAI, Phys. of Fluids, 9, 1634, 1966

65 D.E.ROTHE, Phys. of Fluids 9, 1943, 1966

66 R.E.CENTER, Phys. of Fluids, 10, 8, 1967

67 W.H.ANDERSEN, D.F.HORNIG, Phys. of Fluids 4, 650, 1961

68 A.E.BEYLICH, Phys. of Fluids, Supplement I, I-82, 1969

69 E.GOLDMAN, L.SIROVICH, J.Fluid Mech. 35, 3, 575, 1969

70 T.FUJIMOTO, IV RGD p.223, 1965

71 B.S.TANENBAUM, R.MACDONALD SCOTT, Phys. of Fluids, 9, 1048, 1966

72 M.M.OBERAI, Phys. of Fluids, 8, 826 1965 ; 9, 1634 1966

73 M.M.OBERAI, U.N.SINHA IX RGD 1974

74 G.A.BIRD, J.Fluid Mech., 31, 4, 657, 1968

75 M.SINCLAIR, J.H.de LEEUW, p.319, RGD v.I ed. L.Trilling H.Y.Wachman, New York, London Acad. Press 1969

76 L.N.HARNETT, E.P.MUNTZ, Phys. of Fluids, 15, 565, 1972

77 W.FISZDON, T. PLATKOWSKI, Engineering Transactions 25, 2, 333, 1977

78 T.PLATKOWSKI, Prace IPPT, Warszawa, 1978

79 T.PLATKOWSKI, XI RGD, Paris CEA, p.323, 1979

80 T.PLATKOWSKI, Prace IPTT 7/1981, Warszawa

81 T.PLATKOWSKI, Doctoral dissertation, 1981

82 P.MAUSBACH, Numerical solution of Boltzmann equation for the problem of shock wave in a binary mixture with disparate masses, XII Symposium on Advances Problems and Methods, Błażejewko, 1979

83 P.MAUSBACH, private communication

84 F.G.THEREMISSINE, Doklady Akademii Nauk 5, 185, 1970

85 F.G.THEREMISSINE, V.V.ARISTOV, Doklady Akademii Nauk, 1, 231, 1976

86 K.ABE, H.OGUCHI, VI RGD, ed.L.TRILLING, H.Y.WACHMAN Acad. Press, 1969

87 F.ROBBEN, L.TALBOT, The Phys. of Fluids ,9 ,4 ,633,1966

88 D.E. ROTHE, UTIAS Report 114, 1966

Appendix A

Coefficients entering the functional (2.7)

To make formulae clear we introduce the following notation:

$$\Delta_{kl}(\underline{c},\underline{c}_*) = f_k^+(\underline{c}')f_l^-(\underline{c}_*') - f_k^+(\underline{c})f_l^-(\underline{c}_*)$$

$$\mathcal{D}_{kl}(\underline{c},\underline{c}_*) = \Delta_{kl}(\underline{c},\underline{c}_*) + \Delta_{lk}(\underline{c}_*,\underline{c})$$

and:

$$P_1(\underline{c}^1) = \frac{1}{4}\Big[\int \mathcal{D}_{11}(\underline{c}^1,\underline{c}_*^1)g_{11}\,bdbd\varepsilon d^3c_*^1 + \int \mathcal{D}_{12}(\underline{c}^1,\underline{c}_*^2)g_{12}\,bdbd\varepsilon d^3c_*^2\Big]$$

$$P_2(\underline{c}^2) = \frac{1}{4}\Big[\int \mathcal{D}_{21}(\underline{c}^2,\underline{c}_*^1)g_{21}\,bdbd\varepsilon d^3c_*^1 + \int \mathcal{D}_{22}(\underline{c}^2,\underline{c}_*^2)g_{22}\,bdbd\varepsilon d^3c_*^2\Big]$$

$$P_3(\underline{c}^1) = -\frac{1}{4}\beta\int\Big[\mathcal{D}_{12}(\underline{c}^1,\underline{c}_*^1) + \mathcal{D}_{21}(\underline{c}^1,\underline{c}_*^1)\Big]g_{11}\,bdbd\varepsilon d^3c_*^1$$
$$-\frac{1}{4}\Big[\frac{1}{\beta}\mathcal{D}_{11}(\underline{c}^1,\underline{c}_*^2) + \beta\mathcal{D}_{22}(\underline{c}^1,\underline{c}_*^2)\Big]g_{12}\,bdbd\varepsilon d^3c_*^2$$

$$P_4(\underline{c}^2) = -\frac{1}{4}\int\Big[\beta\mathcal{D}_{22}(\underline{c}^2,\underline{c}_*^1) + \frac{1}{\beta}\mathcal{D}_{11}(\underline{c}^2,\underline{c}_*^1)\Big]g_{21}\,bdbd\varepsilon d^3c_*^1$$
$$-\frac{1}{4}\int\Big[\frac{1}{\beta}\Big\{\mathcal{D}_{21}(\underline{c}^2,\underline{c}_*^2) + \mathcal{D}_{12}(\underline{c}^2,\underline{c}_*^2)\Big\}\Big]g_{22}\,bdbd\varepsilon d^3c_*^2$$

$$P_5(\underline{c}^1) = \frac{1}{4}\int\beta\Big[\Delta_{21}(\underline{c}^1,\underline{c}^1) - \Delta_{12}(\underline{c}^1,\underline{c}_*^1) + \Delta_{21}(\underline{c}^1,\underline{c}_*^1) - \Delta_{12}(\underline{c}_*^1,\underline{c}^1)\Big]g_{11}\,bdbd\varepsilon d^3c_*^1$$
$$+\frac{1}{4}\int\Big\{\frac{1}{\beta}\Big[\Delta_{11}(\underline{c}_*^2,\underline{c}^1) - \Delta_{11}(\underline{c}^1,\underline{c}_*^2)\Big] + \beta\Big[\Delta_{22}(\underline{c}^1,\underline{c}_*^2) - \Delta_{22}(\underline{c}_*^2,\underline{c}^1)\Big]\Big\}g_{12}\,bdbd\varepsilon d^3c_*^2$$

$$P_6(\underline{c}^2) = \frac{1}{4}\Big\{\beta\Big[\Delta_{22}(\underline{c}_*^1,\underline{c}^2) - \Delta_{22}(\underline{c}^2,\underline{c}_*^1)\Big] + \frac{1}{\beta}\Big[\Delta_{11}(\underline{c}^2,\underline{c}_*^1) - \Delta_{11}(\underline{c}_*^1,\underline{c}^2)\Big]\Big\}g_{21}\,bdbd\varepsilon d^3c_*^1$$
$$+\frac{1}{4\beta}\int\Big\{\Delta_{12}(\underline{c}_*^2,\underline{c}^2) - \Delta_{21}(\underline{c}^2,\underline{c}_*^2) + \Delta_{12}(\underline{c}^2,\underline{c}_*^2) - \Delta_{21}(\underline{c}_*^2,\underline{c}^2)\Big\}g_{22}\,bdbd\varepsilon d^3c_*^2$$

$$P_7(\underline{c}^1) = -\frac{1}{4}\beta^2\int \mathcal{D}_{22}(\underline{c}^1,\underline{c}^2_*)\, g_{11}\, b\,db\,d\varepsilon\, d^3c_* - \frac{1}{4}\int \mathcal{D}_{21}(\underline{c}^1,\underline{c}^1_*)\, g_{12}\, b\,db\,d\varepsilon\, d^3c_*$$

$$P_8(\underline{c}^2) = -\frac{1}{4}\int \mathcal{D}_{12}(\underline{c}^2,\underline{c}^1_*)\, g_{21}\, b\,db\,d\varepsilon\, d^3c_* - \frac{1}{4\beta^2}\int \mathcal{D}_{11}(\underline{c}^2,\underline{c}^2_*)\, g_{22}\, b\,db\,d\varepsilon\, d^3c_*$$

and $\beta = \frac{m_2}{m_1} = \beta_{21}$

Finally,

$$A_0 = \int \frac{c_x^2}{4}\left[f_1^+(\underline{c}) - f_1^-(\underline{c})\right] d^3c$$

$$A_{01} = \int \frac{c_x^2}{4}\left[f_2^+(\underline{c}) - f_2^-(\underline{c})\right] d^3c$$

$$A = A_0 + A_{01}$$

$$A_1 = \int \frac{c_x^2}{2}\left[f_1^+(\underline{c}) - f_1^-(\underline{c})\right]\left[f_2^+(\underline{c}) - f_2^-(\underline{c})\right]\left(\beta + \frac{1}{\beta}\right) d^3c$$

$$A_2 = \beta^2 A_{01} + \frac{1}{\beta^2} A_0$$

$$A_3 = \int c_x^1 P_1(\underline{c}^1)\left[f_1^+(\underline{c}^1) - f_1^-(\underline{c}^1)\right] d^3c^1 - \int c_x^2 P_2(\underline{c}^2)\left[f_2^+(\underline{c}^2) - f_2^-(\underline{c}^2)\right] d^3c^2$$

$$A_4 = -A_3$$

$$A_5 = -\int c_x^1 P_3(\underline{c}^1)\left[f_1^+(\underline{c}^1) - f_1^-(\underline{c}^1)\right] d^3c^1 - \int c_x^2 P_4(\underline{c}^2)\left[f_2^+(\underline{c}^2) - f_2^-(\underline{c}^2)\right] d^3c^2$$

$$A_6 = -\int c_x^1 P_5(\underline{c}^1)\left[f_1^+(\underline{c}^1) - f_1^-(\underline{c}^1)\right] d^3c^1 - \int c_x^2 P_6(\underline{c}^2)\left[f_2^+(\underline{c}^2) - f_2^-(\underline{c}^2)\right] d^3c^2$$

$$A_7 = -\int c_x^1 P_7(\underline{c}^1)[f_1^+(\underline{c}^1) - f_1^-(\underline{c}^1)]d^3c^1 - \int c_x^2 P_8(\underline{c}^2)[f_2^+(\underline{c}^2) - f_2^-(\underline{c}^2)]d^3c^2$$

$$A_8 = -\int c_x^1 \beta P_1(\underline{c}^1)[f_2^+(\underline{c}^1) - f_2^-(\underline{c}^1)]d^3c^1 - \int \frac{c_x^2}{\beta} P_2(\underline{c}^2)[f_1^+(\underline{c}^2) - f_1^-(\underline{c}^2)]d^3c^2$$

$$A_9 = -A_8$$

$$A_{10} = -\int c_x^1 \beta P_3(\underline{c}^1)[f_2^+(\underline{c}^1) - f_2^-(\underline{c}^1)]d^3c^1 - \int \frac{c_x^2}{\beta} P_4(\underline{c}^2)[f_1^+(\underline{c}^2) - f_1^-(\underline{c}^2)]d^3c^2$$

$$A_{11} = -\int c_x^1 \beta P_5(\underline{c}^1)[f_2^+(\underline{c}^1) - f_2^-(\underline{c}^1)]d^3c^1 - \int \frac{c_x^2}{\beta} P_6(\underline{c}^2)[f_1^+(\underline{c}^2) - f_1^-(\underline{c}^2)]d^3c^2$$

$$A_{12} = -\int c_x^1 \beta P_7(\underline{c}^1)[f_2^+(\underline{c}^1) - f_2^-(\underline{c}^1)]d^3c^1 - \int \frac{c_x^2}{\beta} P_8(\underline{c}^2)[f_1^+(\underline{c}^2) - f_1^-(\underline{c}^2)]d^3c^2$$

$$A_{13} = \int P_1^2(\underline{c}^1)d^3c^1 + \int P_2^2(\underline{c}^2)d^3c^2$$

$$A_{14} = \int 2P_1(\underline{c}^1)P_5(\underline{c}^1)d^3c^1 + \int 2P_2(\underline{c}^2)P_6(\underline{c}^2)d^3c^2$$

$$A_{15} = \int [P_5^2(\underline{c}^1) + 2P_1(\underline{c}^1)P_7(\underline{c}^1)]d^3c^1 + \int [P_6^2(\underline{c}^2) + 2P_2(\underline{c}^2)P_8(\underline{c}^2)]d^3c^2$$

$$A_{16} = \int 2P_1(\underline{c}^1)P_3(\underline{c}^1)d^3c^1 + \int 2P_2(\underline{c}^2)P_4(\underline{c}^2)d^3c^2$$

$$A_{17} = -A_{14}$$

$$A_{18} = \int 2P_3(\underline{c}^1)P_5(\underline{c}^1)d^3c^1 + \int 2P_4(\underline{c}^2)P_6(\underline{c}^2)d^3c^2$$

$$A_{19} = \int 2P_5(\underline{c}^1)P_7(\underline{c}^1)d^3c^1 + \int 2P_6(\underline{c}^2)P_8(\underline{c}^2)d^3c^2$$

$$A_{20} = \int P_7^2(\underline{c}^1)d^3c^1 + \int P_8^2(\underline{c}^2)d^3c^2$$

$$A_{21} = -A_{16}$$

$$A_{22} = \int 2P_3(\underline{c}^1)P_7(\underline{c}^2)d^3c^1 + \int 2P_7(\underline{c}^2)P_8(\underline{c}^2)\,d^3c^2$$

$$A_{23} = \int [P_3^2(\underline{c}^1) - 2P_1(\underline{c}^1)P_7(\underline{c}^1)]\,d^3c^1 + \int [P_7^2(\underline{c}^2) - 2P_2(\underline{c}^2)P_8(\underline{c}^2)]d^3c^2$$

In the case of a monatomic one-component gas the functional S (2.4) reduces to (2.10) with coefficients:

$$A = \int \frac{c_*^2}{4}[f^+(\underline{c}) - f^-(\underline{c})]^2 d^3c$$

$$B = \int \frac{c_*(f^+ - f^-)}{4}\{f^-(\underline{c}')f^+(\underline{c}_*') - f^-(\underline{c})f^+(\underline{c}_*) + f^+(\underline{c}')f^-(\underline{c}_*') - f^+(\underline{c})f^-(\underline{c}_*)\} g b db d\varepsilon d^3c_* d^3c$$

$$C = \frac{1}{16}\int \{[f^-(\underline{c}')f^+(\underline{c}_*') - f^-(\underline{c})f^+(\underline{c}_*) + f^+(\underline{c}')f^-(\underline{c}_*') - f^+(\underline{c})f^-(\underline{c}_*)]\, g b db d\varepsilon d^3c_*\}^2 d^3c$$

where

$$g = |\underline{c}_* - \underline{c}|$$

Appendix B

Functions entering the differential equations (5.4)

Let us introduce the following notation :

$\varphi(x) = \frac{x^{\iota}}{x^{\iota+1}} \operatorname{sgn} x$, here ι - natural even number

$\tilde{\varphi}(x) = x\alpha(x)$

$\alpha(x) = x\varphi(x)$

$\tilde{f}(x) = -2\alpha(x)\alpha(x) = -2\alpha(x)x\varphi(x)$

$F_1(x) = \tilde{f}' \exp\tilde{f}$

$F_2(x) = \frac{\tilde{\varphi}'}{ch^2[x\alpha(x)]}$

$F_3(x) = (\tilde{f}'' + \tilde{f}'^2)\exp\tilde{f}$

$F_4(x) = -2ch^{-3}[\tilde{\varphi}(x)]\operatorname{sh}[\tilde{\varphi}(x)]\tilde{\varphi}'(x)^2 + ch^{-2}[\tilde{\varphi}(x)]\tilde{\varphi}''(x)$

Then the coefficients appearing in (5.4) are:

$G_1 = -2A\exp\tilde{f}$

$G_2 = -A_1\exp\tilde{f}$

$G_3 = -4AF_1$

$G_4 = -2A_1F_1 + \exp(2\tilde{f})(2A_9 - A_5)y + \exp\tilde{f}(2A_9 - A_5)\operatorname{th}[\tilde{\varphi}(x)] +$
$+ \exp(2\tilde{f})(A_{10} - 2A_7)\tilde{y} - \exp\tilde{f}A_6$

$G_{00} = -2AF_4 - 4A_{13}\operatorname{th}\tilde{\varphi} + 4A_{13}\operatorname{th}^3\tilde{\varphi}$

$G_{10} = -2AF_3 - 4A_{13}\exp\tilde{f} + 12A_{13}\operatorname{th}^2\tilde{\varphi}\exp\tilde{f}$

$G_{01} = -A_1F_3 + F_1(2A_9 - A_5)\operatorname{th}\tilde{\varphi} - A_6F_1 + A_{16}\exp\tilde{f} - 3A_{16}\operatorname{th}^2\tilde{\varphi}\exp\tilde{f}$
$- 2A_{11}\operatorname{th}\tilde{\varphi}\exp\tilde{f}$

$G_{20} = 12A_{13}\operatorname{th}\tilde{\varphi}\exp(2\tilde{f})$

$G_{02} = (A_{10} - 2A_7)F_1\exp\tilde{f} + A_{18}\exp(2\tilde{f}) + 2A_{15}\operatorname{th}\tilde{\varphi}\exp(2\tilde{f})$

$G_{11} = (2A_9 - A_5)F_1\exp\tilde{f} - 6A_{16}\operatorname{th}\tilde{\varphi}\exp(2\tilde{f}) - 2A_{14}\exp(2\tilde{f})$

$G_{30} = 4A_{13}\exp(3\tilde{f})$

$$G_{03} = A_{22}\exp(3\tilde{f})$$

$$G_{21} = -3A_{16}\exp(3\tilde{f})$$

$$G_{12} = 2A_{23}\exp(3\tilde{f})$$

$$H_1 = -A_1\exp\tilde{f}$$

$$H_2 = -2A_2\exp\tilde{f}$$

$$H_3 = -2A_1F_1 - (2A_9-A_5)\exp(2\tilde{f})y + A_6\exp(\tilde{f}) - (2A_9-A_5)\mathrm{th}[\tilde{\varphi}(x)]\exp\tilde{f} - (A_{10}-2A_7)\exp(2\tilde{f})\tilde{y}$$

$$H_4 = -4A_2F_1$$

$$H_{00} = -A_1F_4 + F_2A_6 - F_2(2A_9-A_5)\mathrm{th}[\tilde{\varphi}(x)] + A_{14} + A_{16}\mathrm{th}[\tilde{\varphi}(x)] - A_{16}\mathrm{th}^3[\tilde{\varphi}(x)] - A_{14}\mathrm{th}^2[\tilde{\varphi}(x)]$$

$$H_{10} = -A_1F_3 - [2A_9-A_5)F_1\mathrm{th}[\tilde{\varphi}(x)] + A_{16}\exp\tilde{f} + A_6F_1 - 3A_{16}\mathrm{th}^2[\tilde{\varphi}(x)]\exp\tilde{f} - 2A_{14}\mathrm{th}[\tilde{\varphi}(x)]\exp\tilde{f} - (2A_9-A_5)F_2\exp\tilde{f}$$

$$H_{01} = -2A_2F_3 - (A_{10}-2A_7)F_2\exp\tilde{f} + 2A_{15}\exp\tilde{f} + 2A_{18}\mathrm{th}[\tilde{\varphi}(x)]\exp\tilde{f} + 2A_{23}\mathrm{th}^2[\tilde{\varphi}(x)]\exp\tilde{f}$$

$$H_{20} = -F_1(2A_9-A_5)\exp\tilde{f} - 3A_{16}\mathrm{th}[\tilde{\varphi}(x)]\exp(2\tilde{f}) - A_{14}\exp(2\tilde{f})$$

$$H_{02} = 3A_{19}\exp(2\tilde{f}) + 3A_{22}\mathrm{th}[\tilde{\varphi}(x)]\exp(2\tilde{f})$$

$$H_{11} = F_1(A_{10}-2A_7)\exp\tilde{f} + 2A_{18}\exp(2\tilde{f}) + 4A_{23}\mathrm{th}[\tilde{\varphi}(x)]\exp(2\tilde{f})$$

$$H_{30} = -A_{16}\exp(3\tilde{f})$$

$$H_{03} = 4A_{20}\exp(3\tilde{f})$$

$$H_{21} = 2A_{23}\exp(3\tilde{f})$$

$$H_{12} = 3A_{22}\exp(3\tilde{f})$$

$$H_{13} = G_{13} = 0 \qquad H_{31} = G_{31} = 0$$

$$H_{22} = G_{22} = 0 \qquad H_{32} = G_{32} = 0$$

$$H_{23} = G_{23} = 0 \qquad H_{33} = G_{33} = 0$$

Appendix C

The parameters characterizing the gas mixture far in front of the shock wave and far behind the shock wave are linked by the Rankine-Hugoniot conditions (6.1) - (6.3) having the same form as for a one-component gas.
Only instead of a relation $\hat{v}^- = \sqrt{\gamma} M^-/2$ there is $\hat{v}^- = \sqrt{\gamma} M^- / \{2[1+W(\beta-1)][1+\frac{1}{\beta}]\}$, where W is a mole fraction of the heavy component in the binary gas mixture at $-\infty$, $W = \frac{n_2^-}{n^-} = \frac{n_2^-}{n_1^- + n_2^-}$ and where $\beta = \frac{m_2}{m_1}$.

Similarly, as in section 6 the solution of one-dimensional Boltzmann equation for a Lennard-Jones (S_2-S_1) potential for a shock wave in the binary gas mixture can be written in terms of the parameters at $-\infty$:

$$(C.1)\quad f_i(\underline{c}, x; n_1^-, n_2^-, T^-, v^-, m_1, m_2, \epsilon_1, \epsilon_2, \epsilon_{12}, \sigma_1, \sigma_2, \sigma_{12}) = n^- \left(\frac{2k}{\mu} T^-\right)^{-3/2} \hat{f}_i(\hat{\underline{c}}, \hat{x}; \hat{n}^-, W, \beta, M^-, \hat{\epsilon}_1, \hat{\epsilon}_2, \hat{\epsilon}_{12}, \hat{\sigma}_1, \hat{\sigma}_2),$$

where $\hat{\sigma}_1 = \frac{\sigma_1}{\sigma_{12}}$, $\hat{\sigma}_2 = \frac{\sigma_2}{\sigma_{12}}$

and where the non-dimensional parameters are dashed and are defined:

$$(C.2)\quad \hat{x} = \frac{x}{\sigma_{12}}; \quad \hat{\underline{c}} = \sqrt{\frac{\mu}{2kT^-}}\,\underline{c}, \quad \hat{\underline{v}} = \sqrt{\frac{\mu}{2kT^-}}\,\underline{v}, \quad \hat{n} = n\sigma_{12}^3,$$

$$\hat{\epsilon} = \frac{\epsilon}{kT^-}, \quad \text{where } \mu = \frac{m_1 m_2}{m_1 + m_2}$$

Taking into account (C.1) and (C.2) from dimensional analysis one obtains:

$$(C.3)\quad \left(\frac{dn}{dx}\right)_{max} = \left(\frac{dn_1}{dx}\right)_{max} + \left(\frac{dn_2}{dx}\right)_{max} = \frac{n^-}{\sigma_{12}} \hat{F}(\hat{n}^-, M^-, W, \beta, \hat{\epsilon}_1, \hat{\epsilon}_2, \hat{\epsilon}_{12}, \hat{\sigma}_1, \hat{\sigma}_2) =$$
$$= (n^-)^2 \sigma_{12}^2 \hat{F}(\hat{n}^-, M^-, W, \beta, \hat{\epsilon}_1, \hat{\epsilon}_2, \hat{\epsilon}_{12}, \hat{\sigma}_1, \hat{\sigma}_2)$$

The Prandtl's shock wave thickness is:

$$(C.4)\quad \Lambda = \frac{\rho^+ - \rho^-}{\left(\frac{d\rho}{dx}\right)_{max}} = \frac{n^+ - n^-}{\left(\frac{dn}{dx}\right)_{max}} = \frac{H_m(M^-) - 1}{n^- \sigma_{12}^2 \hat{F}(\hat{n}^-, M^-, W, \beta, \hat{\epsilon}_1, \hat{\epsilon}_2, \hat{\epsilon}_{12}, \hat{\sigma}_1, \hat{\sigma}_2)} =$$

$$= \frac{\sigma_{12}\,[H_m(M^-) - 1]}{\hat{n}^- \hat{F}(\hat{n}^-, M^-, W, \beta, \hat{\epsilon}_1, \hat{\epsilon}_2, \hat{\epsilon}_{12}, \hat{\sigma}_1, \hat{\sigma}_2)}$$

As in (6.9) the mean free path at $-\infty$ for the binary gas mixture is:

$$(C.5)\quad \lambda^- = \frac{1}{\pi n^- \sigma_{12}^2} \left[\frac{(1-W)}{\sqrt{2}\,(1-W)\,\hat{\sigma}_1^2\,\Omega^{(1,1)^*}(\hat{\epsilon}_1) + \frac{W}{4}\,\Omega^{(2,2)^*}(\hat{\epsilon}_{12})\left\{1 + \frac{1}{\beta}\right\}^{1/2}} \right.$$

$$\left. + \frac{W}{\sqrt{2}\,W\,\hat{\sigma}_2^2\,\Omega^{(2,2)^*}(\hat{\epsilon}_2) + \frac{1-W}{4}\,\Omega^{(2,2)^*}(\hat{\epsilon}_{12})\left\{1 + \beta\right\}^{1/2}} \right] =$$

$$= \frac{1}{n^- \sigma_{12}^2}\, \hat{\mathcal{L}}(W, \beta, \hat{\epsilon}_1, \hat{\epsilon}_2, \hat{\epsilon}_{12}, \hat{\sigma}_1, \hat{\sigma}_2)$$

Hence in general case:

$$(C.6)\quad \frac{\Lambda}{\lambda^-} = \frac{[\,H_m(M^-) - 1\,]}{\hat{F}(\hat{n}^-, M^-, W, \beta, \hat{\epsilon}_1, \hat{\epsilon}_2, \hat{\epsilon}_{12}, \hat{\sigma}_1, \hat{\sigma}_2)\,\hat{\mathcal{L}}(W, \beta, \hat{\epsilon}_1, \hat{\epsilon}_2, \hat{\epsilon}_{12}, \hat{\sigma}_1, \hat{\sigma}_2)}$$

$$= \hat{\mathcal{L}}_0(\hat{n}^-, M^-, W, \beta, \hat{\epsilon}_1, \hat{\epsilon}_2, \hat{\epsilon}_{12}, \hat{\sigma}_1, \hat{\sigma}_2)$$

Introducing non-dimensional variables (C.2) we can write:

$$(C.7)\quad f_1^+(\underline{c}) = n^- \left(\frac{2kT^-}{\mu}\right)^{-3/2} (1-W)\, H_m(M^-) \left\{\pi H_T(M^-)\right\}^{-3/2} \left(1 + \frac{1}{\beta}\right) \cdot$$

$$\exp\left\{-(1+\beta)\frac{[\hat{c} - \hat{x}^- H_x(M^-)]^2}{H_T(M^-)}\right\} = n^- \left(\frac{2kT^-}{\mu}\right)^{-3/2} \hat{f}^+(\hat{\underline{c}})$$

$$f_1^-(\underline{c}) = n^-\left(\frac{2kT^-}{\mu}\right)^{-3/2}(1-w)\pi^{-3/2}\left(1+\frac{1}{\beta}\right)^{3/2}\exp\left[-\left(1+\frac{1}{\beta}\right)(\hat{\underline{c}}-\hat{\underline{v}}^-)^2\right] =$$

$$= n^-\left(\frac{2kT^-}{\mu}\right)^{-3/2}\hat{f}^-(\hat{\underline{c}})$$

$$f_2^+(\underline{c}) = n^-\left(\frac{2kT^-}{\mu}\right)^{-3/2} w\, H_m(M^-)\left[\pi H_T(M^-)\right]^{-3/2}(1+\beta)^{3/2}\exp\left\{-(1+\beta)\frac{[\hat{\underline{c}}-\hat{\underline{v}}^- H_v(M^-)]^2}{H_T(M^-)}\right\}$$

$$= n^-\left(\frac{2kT^-}{\mu}\right)^{-3/2} f_2^+(\hat{\underline{c}})$$

$$f_2^-(\underline{c}) = n^-\left(\frac{2kT^-}{\mu}\right)^{-3/2} w\,\pi^{-3/2}(1+\beta)^{3/2}\exp\left[-(1+\beta)(\hat{\underline{c}}-\hat{\underline{v}}^-)^2\right] =$$

$$= n^-\left(\frac{2kT^-}{\mu}\right)^{-3/2}\hat{f}_2^-(\hat{\underline{c}})$$

where: $\hat{v}^- = \dfrac{\sqrt{\delta}\,M^-}{\sqrt{2[1+w(\beta-1)](1+\frac{1}{\beta})^3}}$

Finally from (C.7) and (4.4), (4.9) it follows that:

$$(C.8)\qquad \alpha_1 = \frac{1}{2}\sqrt{\frac{-B_1+\sqrt{B_1^2-4B_0B_2}}{2B_0}} = n^-\sigma_{12}^2\hat{\alpha}_1(M^-,w,\beta,\hat{\epsilon}_1,\hat{\epsilon}_2,\hat{\epsilon}_{12},\hat{\sigma}_1,\hat{\sigma}_2)$$

and

$$(C.9)\qquad \alpha_2 = \frac{1}{2}\sqrt{\frac{C_1+\sqrt{C_1^2-4C_0C_2}}{2C_0}} = n^-\sigma_{12}^2\hat{\alpha}_2(M^-,w,\beta,\hat{\epsilon}_1,\hat{\epsilon}_2,\hat{\epsilon}_{12},\hat{\sigma}_1,\hat{\sigma}_2)$$

(C.8) and (C.9) and (C.5) lead to:

$$(C.10)\qquad \lambda^-\alpha_1 = \hat{L}_1(M^-,w,\beta,\hat{\epsilon}_1,\hat{\epsilon}_2,\hat{\epsilon}_{12},\hat{\sigma}_1,\hat{\sigma}_2)$$

$$(C.11)\qquad \lambda^-\alpha_2 = \hat{L}_2(M^-,w,\beta,\hat{\epsilon}_1,\hat{\epsilon}_2,\hat{\epsilon}_{12},\hat{\sigma}_1,\hat{\sigma}_2)$$

and for the shock wave thickness in the binary gas mixture based on a description of the shock wave relaxation :

$$(C.12)\qquad \frac{\Lambda^*}{\lambda^-} = \frac{1}{\lambda^-}\frac{4}{(\alpha_1+\alpha_2)} = \hat{L}(M^-,w,\beta,\hat{\epsilon}_1,\hat{\epsilon}_2,\hat{\epsilon}_{12},\hat{\sigma}_1,\hat{\sigma}_2)$$

For point centers of repulsion potentials (6.23), which can describe the interaction between the molecules of the same gas:

$$(C.13)\qquad \Phi_1 = \tilde{\varepsilon}_1 \left(\frac{\sigma_1}{r}\right)^s \quad , \quad \Phi_2 = \tilde{\varepsilon}_2 \left(\frac{\sigma_2}{r}\right)^s$$

and the molecules of different gases:

$$(C.14)\qquad \Phi_{12} = \tilde{\varepsilon}_{12} \left(\frac{\sigma_{12}}{r}\right)^s ,$$

we introduce instead of $\sigma_1, \sigma_2, \sigma_{12}$ respectively:

$$(C.15)\qquad \tilde{\sigma}_1 = \sigma_1 \left(\frac{\tilde{\varepsilon}_1}{kT}\right)^{1/s} \quad , \quad \tilde{\sigma}_2 = \sigma_2 \left(\frac{\tilde{\varepsilon}_1}{kT}\right)^{1/s} \quad , \quad \tilde{\sigma}_{12} = \sigma_{12} \left(\frac{\tilde{\varepsilon}_{12}}{kT}\right)^{1/s}$$

Similarly to (C.2) the non-dimensional parameters are defined:

$$(C.16)\qquad \hat{x} = \frac{x}{\tilde{\sigma}_{12}} \quad , \quad \underline{\hat{c}} = \sqrt{\frac{\mu}{2kT}}\,\underline{c} \quad , \quad \underline{\hat{v}} = \sqrt{\frac{\mu}{2kT}}\,\underline{v} \quad , \quad \hat{n} = n\tilde{\sigma}_{12}^3$$

An analogous approach, as for the Lennard-Jones potential, leads to the conclusion:

$$(C.17)\qquad \alpha_1 = n^- \tilde{\sigma}_{12}^2 \tilde{\hat{\alpha}}_1 (M^-, w, \beta, \hat{\sigma}_1, \hat{\sigma}_2)$$

$$(C.18)\qquad \alpha_2 = n^- \tilde{\sigma}_{12}^2 \tilde{\hat{\alpha}}_2 (M^-, w, \beta, \hat{\sigma}_1, \hat{\sigma}_2)$$

The mean free path at $-\infty$ in the case of point centers of repulsion potential and for one-component gas is as (6.25):

$$\lambda^- = \left[\frac{\sqrt{2}}{2}\pi n^- \sigma^2 \tilde{A}_2(s)\Gamma\left(4-\frac{2}{s}\right)\left(\frac{s\tilde{\varepsilon}}{kT}\right)^{2/s}\right]^{-1} = \left[\frac{\sqrt{2}}{2}\pi n^- \tilde{\sigma}^2 \tilde{A}_2(s)\Gamma\left(4-\frac{2}{s}\right)s^{2/s}\right]^{-1} =$$

$$(C.19)\qquad = \left[\sqrt{2}\,\pi n^- \tilde{\sigma}^2 \Omega(s)\right]^{-1}$$

and for binary gas mixture is:

$$(c.20)\quad \lambda^{-} = \frac{1}{\pi n^{-} \tilde{\sigma}_{12}^{2} \Omega(s)} \left[\frac{1-w}{\sqrt{2}(1-w)\hat{\sigma}_1 + \frac{w}{4}\left\{1+\frac{1}{\beta}\right\}^{1/2}} + \frac{w}{\sqrt{2}w\hat{\sigma}_2 + \frac{1-w}{4}\left\{1+\beta\right\}^{1/2}} \right]$$

Finally:

$$(c.21)\quad \lambda^{-}\alpha_1 = \hat{\ell}_1(M^{-}, w, \beta, \hat{\sigma}_1, \hat{\sigma}_2)$$

$$(c.22)\quad \lambda^{-}\alpha_2 = \hat{\ell}_2(M^{-}, w, \beta, \hat{\sigma}_1, \hat{\sigma}_2)$$

and also the ratio of "relaxation thickness" of the shock wave to the mean free path is a function only of $M^{-}, w, \beta, \hat{\sigma}_1, \hat{\sigma}_2$:

$$(c.23)\quad \frac{\Lambda^{*}}{\lambda^{-}} = \frac{1}{\lambda^{-}}\left(\frac{4}{\alpha_1+\alpha_2}\right) = \hat{\ell}(M^{-}, w, \beta, \hat{\sigma}_1, \hat{\sigma}_2)$$

Notation

$A, B, C, A_1, \dots A_{25}$ coefficients defined in Appendix A) (2.7), (2.10)

A_j, B_j, C_j - matrices defined in 5 - section 5

χ_2 - function defined in 6 and [18,55]

a_s - asymmetry coefficient

$a_1, \tilde{a}_1, b_1, \tilde{b}_1, B_0, B_1, B_2, C_0, C_1, C_2$ constants defined in 4

b - the impact parameter

$\underline{c}, \underline{c}_*, \underline{c}', \underline{c}_*'$ - respectively: velocity vectors of the pair of the colliding molecules before and after collision

$\underline{c} = [c_x, c_y, c_z] = [c_r \sin\tilde{\theta}\cos\tilde{\omega}, c_r \sin\tilde{\theta}\sin\tilde{\omega}, c_r \cos\tilde{\theta}]$

C_{Ar}, C_{Xe} - mass concentration of heavier component of gas mixture (resp. argon, xenon)

$\underline{e}_x, \underline{e}_y, \underline{e}_z$ versors in x, y, z coordinate system

f - velocity distribution function

$\hat{F}, \hat{G}$ - functions defined in 6

F_j^i - vector defined in 5

$\underline{g} = \underline{c}_* - \underline{c}$ the intial relative velocity vector of the pair of molecules

$G_1, \dots G_4, G_j^i$ - functions specified in Appendix B; section 5

$h(x), \bar{h}(x)$ auxiliary functions defined by (2.5) and (2.6)

$H_1, \dots H_9, H_j^i$ functions specified in Appendix B ; section 5

H_n, H_T, H_V functions defined in 6

k - Boltzmann constant

$\underline{k}$ - unit apse vector

m - molecular mass

M - Mach number

n - number density

$\underline{n}_c$ - unit normal vector to the collision plane

$\underline{n}_e$ - unit normal vector to $(x, \underline{g})$ plane

$\underline{n}_g$ - unit vector perpendicular to $\underline{g}$ and lying on the collision plane

p - pressure

r, θ - polar coordinates

r_{min} - defined in 3

$R = \frac{k}{m}$

S - functional defined by (2.4)

s - index of repulsion

s_1 - index of repulsion, s_2 index of attraction

δ_{loc} - local error

T - temperature

v - velocity

x - distance along direction of flow

$\tilde{\chi} = \tilde{\beta}_0 - \tilde{\beta}$

X^i_j - matrix defined in 5

$y(x), \tilde{y}(x), Y(x), \tilde{Y}(x)$ - auxiliary functions defined resp. in 5, 4

Y^i_j, Z^i_j - vectors defined in 5

$\alpha_1, \alpha_2 (\mathcal{X}_1, \mathcal{X}_2), \alpha$ relaxation parameters

β - the ratio of molecular masses

$\tilde{\beta} = \frac{b}{r}$, $\tilde{\beta}_0 = \frac{b}{r_{min}}$ defined in 3

δ_{glob}, δ_{loc} - respectively: the relative global and local errors characterizing the accuracy of the method

ε - the azimuthal angle

ϵ - the depth of the potential well (potential parameter)

$\Phi(r)$ - intermolecular potential

$\varphi(x), \tilde{\varphi}(x)$ - functions defined in Appendix B

γ - isentropic index

χ_{ij} - collision integrals ($\chi_1 = \chi_{11} + \chi_{12}$, $\chi_2 = \chi_{21} + \chi_{22}$), (2.1)

Λ - thickness of the shock wave (Prandtl's definition)

Λ^* "relaxation" thickness for the shock wave

μ - the reduced mass of the pair of colliding molecules

W - mole fraction of heavier component

$\Omega^{(2,2)*}$ - function - integral - defined in 4 [18]

σ - potential parameter (the value of r for which $\Phi(r) = 0$)

$\tilde{\sigma}$ - parameter defined in 6

Υ - the impact angle

Reduced parameters

$$\bar{n} = \frac{n - n^-}{n^+ - n^-}, \quad \bar{T} = \frac{T - T^-}{T^+ - T^-}, \quad \bar{v} = \frac{v - v^+}{v^- - v^+}$$

dimensionless parameters:

$$\hat{x} = \frac{x}{\sigma}, \quad \hat{\underline{\zeta}} = \sqrt{\frac{\mu}{2kT}}\,\underline{\zeta}, \quad \hat{\underline{v}} = \sqrt{\frac{\mu}{2kT}}\,\underline{v}, \quad \hat{n} = n\sigma^3, \quad \hat{\epsilon} = \frac{\epsilon}{kT}, \quad \hat{\Phi} = \frac{\Phi}{kT}$$

i, j - denote components of gas mixture

Superscripts

$+$ ——— $+\infty$, far behind the shock wave

$-$ ——— $-\infty$, far in front of the shock wave

Subscripts

$*$ notation applied for the second molecule colliding with first one

Ar argon

He helium

Xe xenon

M mixture

ONE-BODY PROBLEM

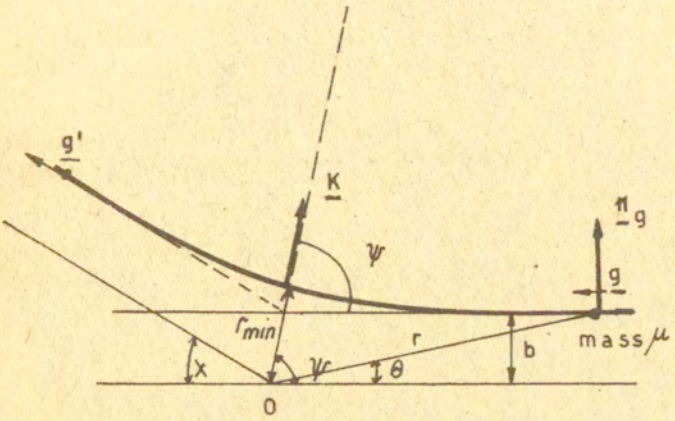

Fig. 1. One-body problem. Collision plane.

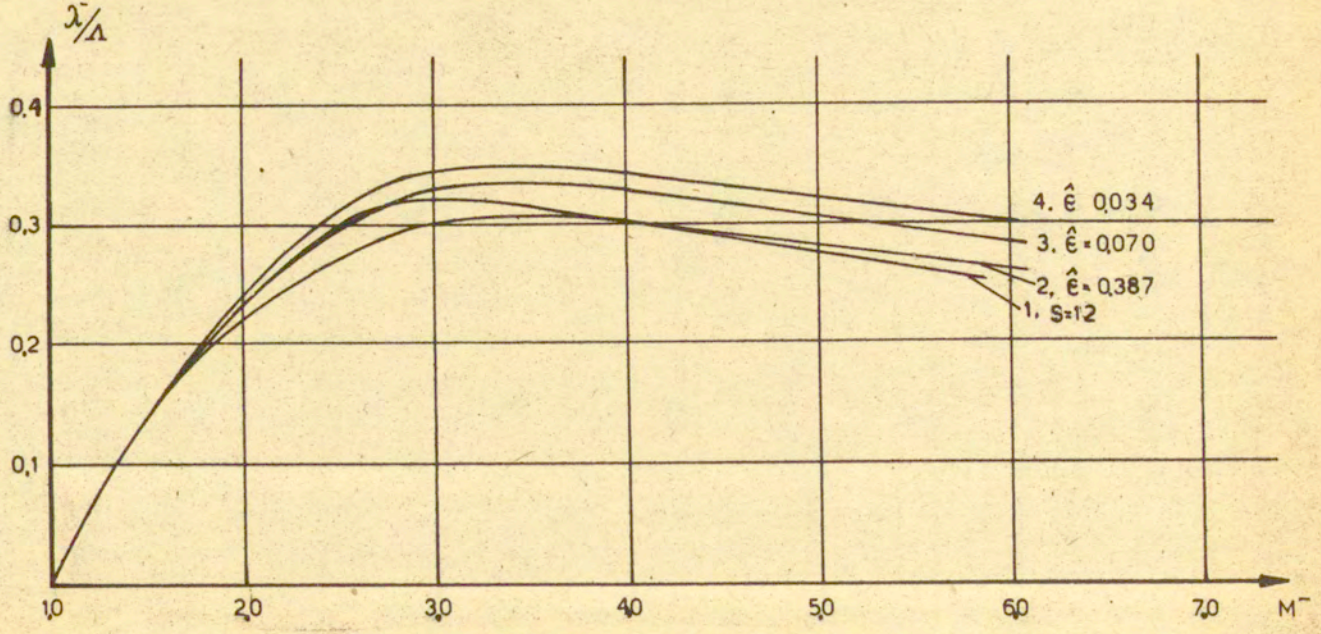

Fig.2. $\frac{\lambda^-}{\Lambda}$ versus M^- (Mach number in front of the shock wave) for the Lennard-Jones (6-12) potential and point centers of repulsion potential. 1-the point centers of repulsion potential - $S = 12$; 2 - L - J, $\hat{\epsilon} = 0.387$, 3-L-J - $\hat{\epsilon} = 0.07$; 4 L-J- $\hat{\epsilon} = 0.034$.

Fig.3 The comparison between the present results and theoretical results of the other authors. $\frac{\lambda^-}{\Lambda}$ versus Mach number in front of the shock wave. 1-the rigid sphere model, Mott-Smith (c_x^3) [10,11]; 2-the rigid sphere model, this work; 3-the rigid sphere model, Mott-Smith (c_x^3) approach, Muckenfuss [11]; 4-the point centers of repulsion potential - s= 12, Mott-Smith (c_x^1) approach, Muckenfuss [11]; 5- s= 12, this work; 6-Maxwellian molecules-s=4, Mott-Smith (c_x^2) approach, Muckenfuss [11]; 7- s=4, this work .

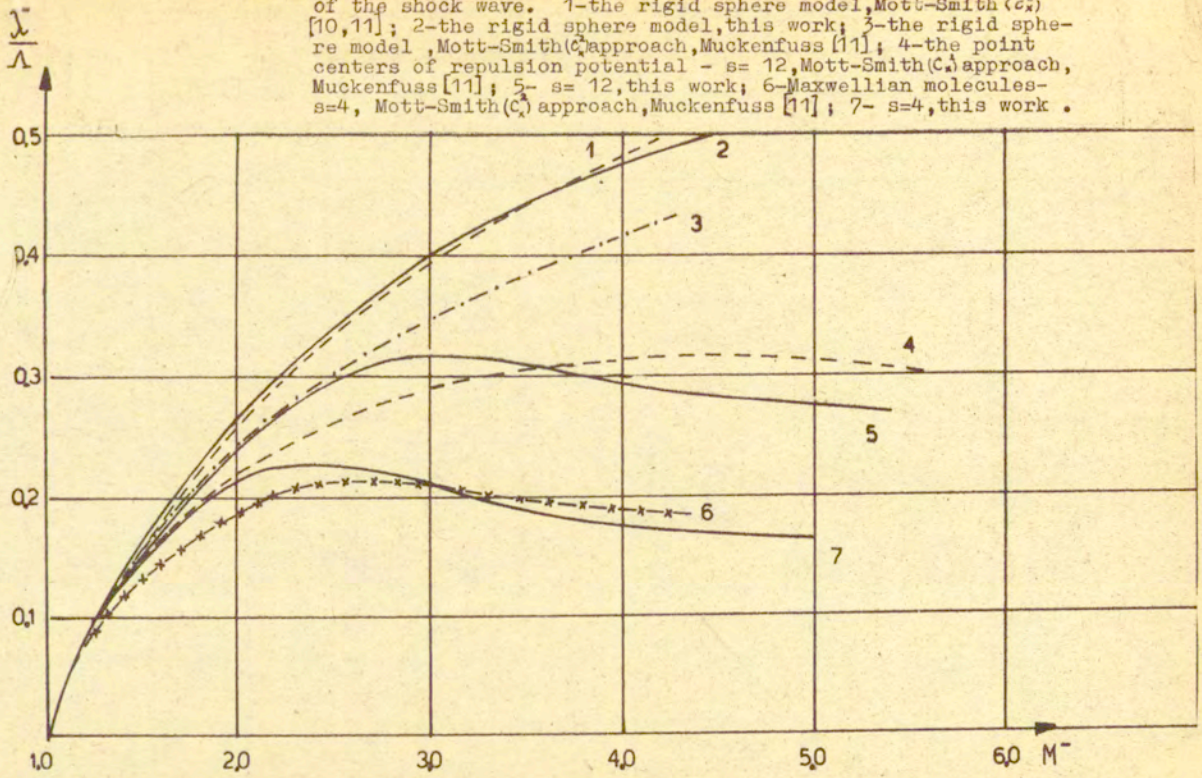

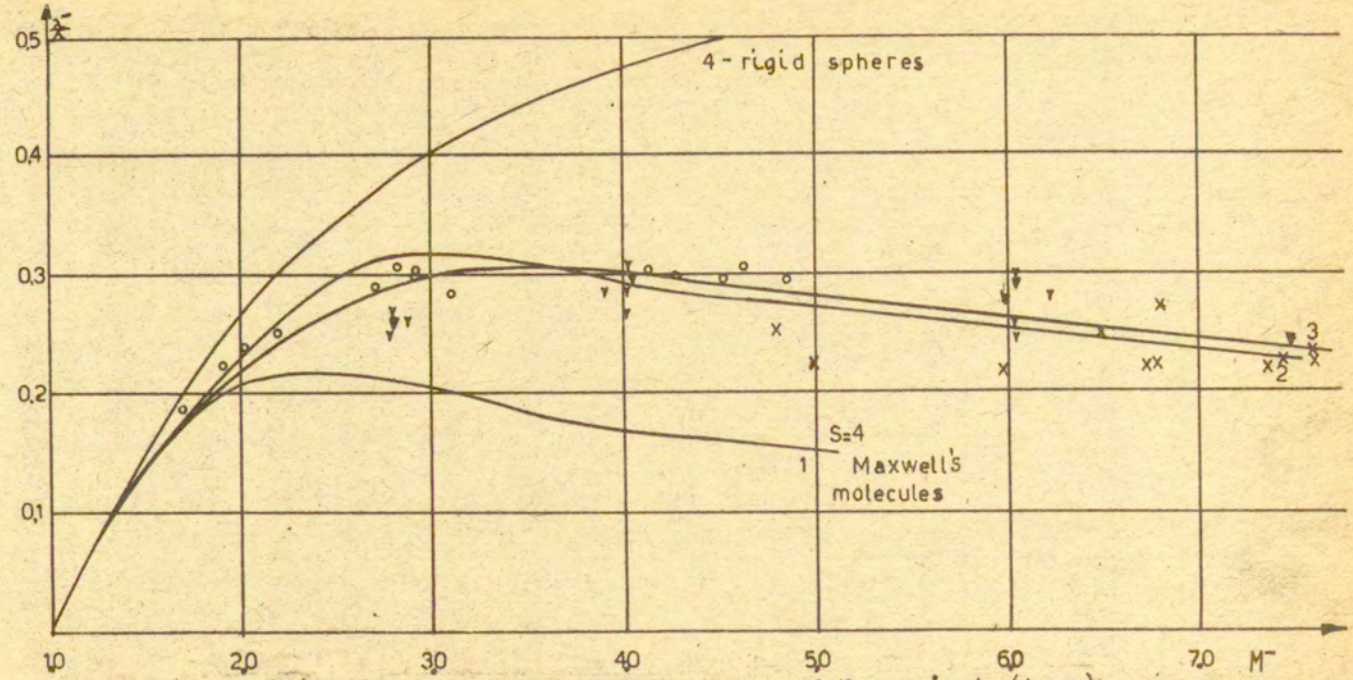

Fig 4. The comparison between the theory and the experiment (Argon); $\frac{\rho}{\rho_\infty}$ versus Mach number in front of the shock wave; theoretical curves: 1 - Maxwell molecules - $s = 4$; 2-the point centers of repulsion potential - $s = 12$; 3-the Lennard-Jones (6-12) potential - $\delta = 0{,}387$; 4-the rigid sphere model; experimental points: ▼ B.Schmidt [42], ○ M.Linzer & D.F.Hornig [49], × M.Camac [45].

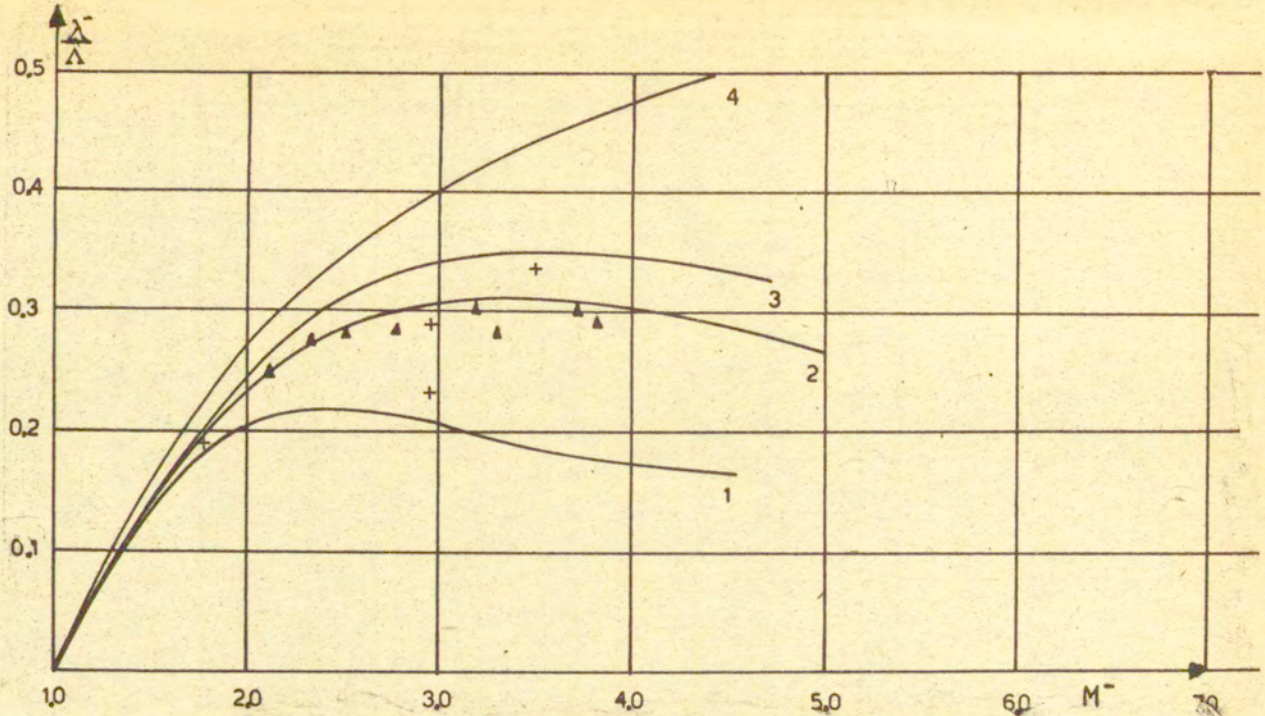

Fig. 5. The comparison between the theory and the experiment (Helium); theoretical curves: 1-Maxwellian molecules, $s = 4$; 2-Lennard-Jones (6-9) potential, $\hat{\varepsilon} = 0.034$; 3-Lennard-Jones (6-12) potential, $\hat{\varepsilon} = 0.034$; 4-rigid spheros model; experimental points: ▲ E.Rieutord [48], + Robben & Talbot [87].

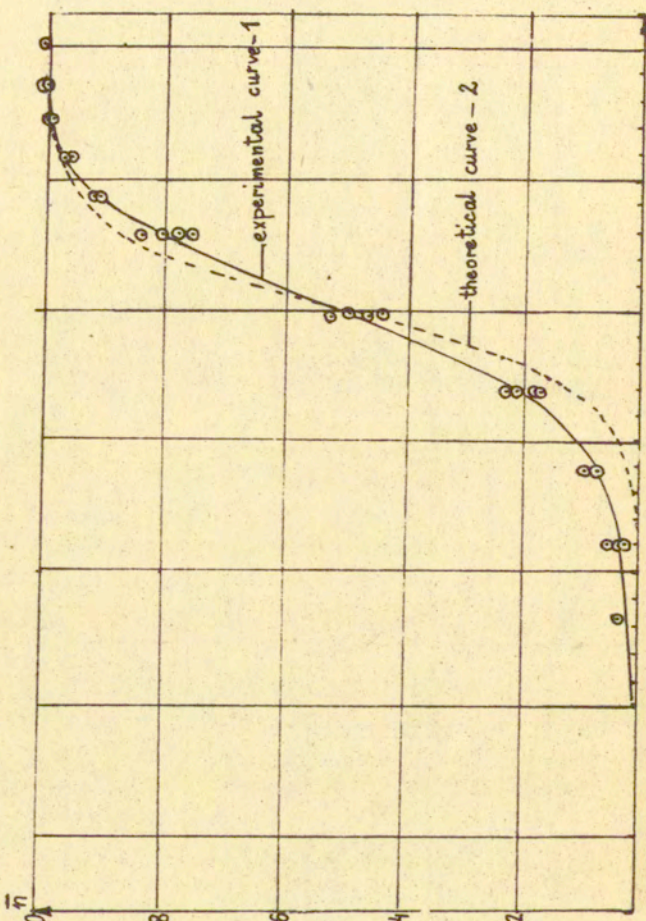

Fig. 6a. The comparison between the theory and the experiment (Argon). The number density distribution within the shock wave; 1-experiment T.Holtz [51], 2-our results.

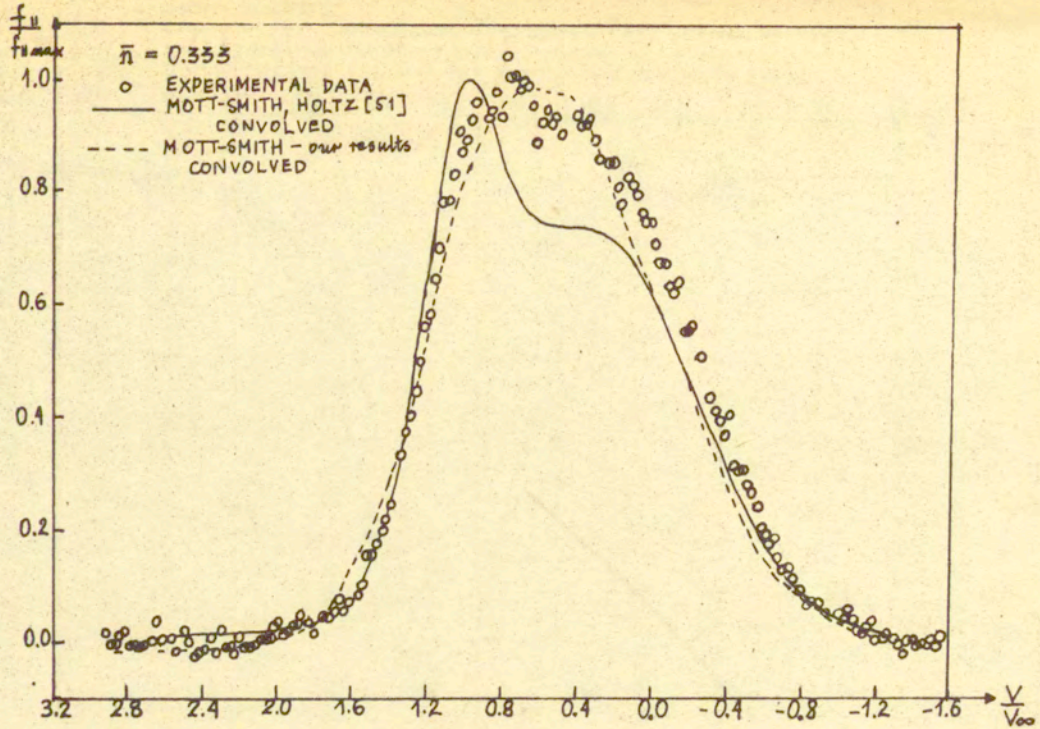

Fig. 6b. The comparison between the theory and the experiment. The normalized parallel velocity distribution function $f_{\parallel}$ (convolved) in the shock wave for $\bar{n} = 0.333$ (1-T.Holtz [51], 2-our results). Notation as in [51].

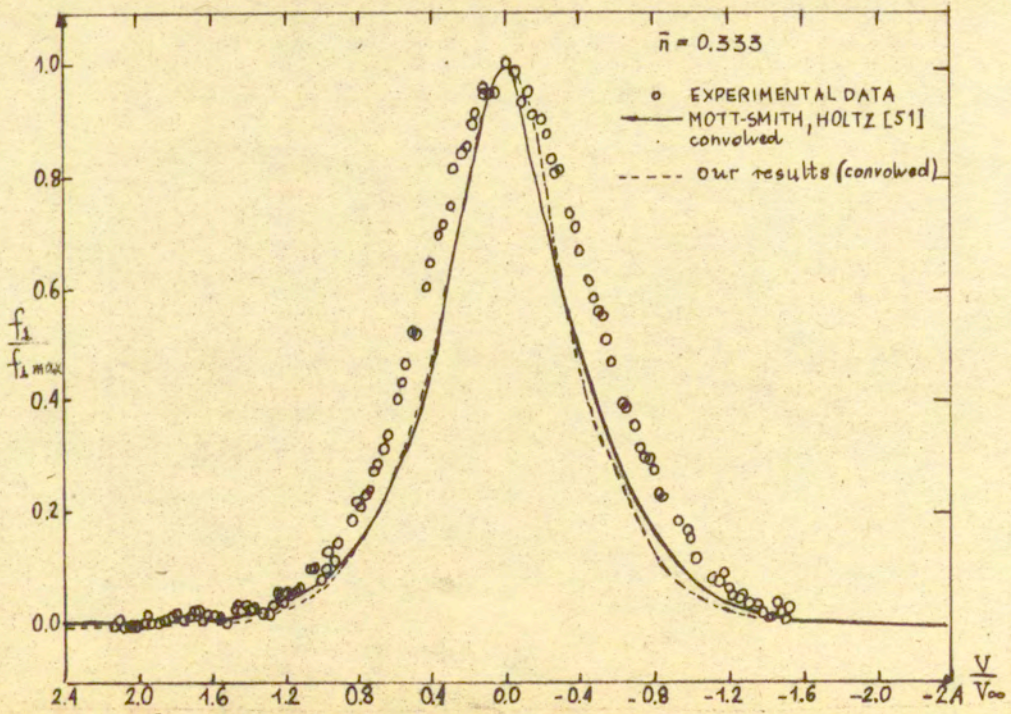

Fig. 6c. The comparison between the theory and the experiment. The normalized perpendicular velocity distribution function $f_\perp$ (convolved) (1-T.Holtz [51], 2-our results). Notation as in [51].

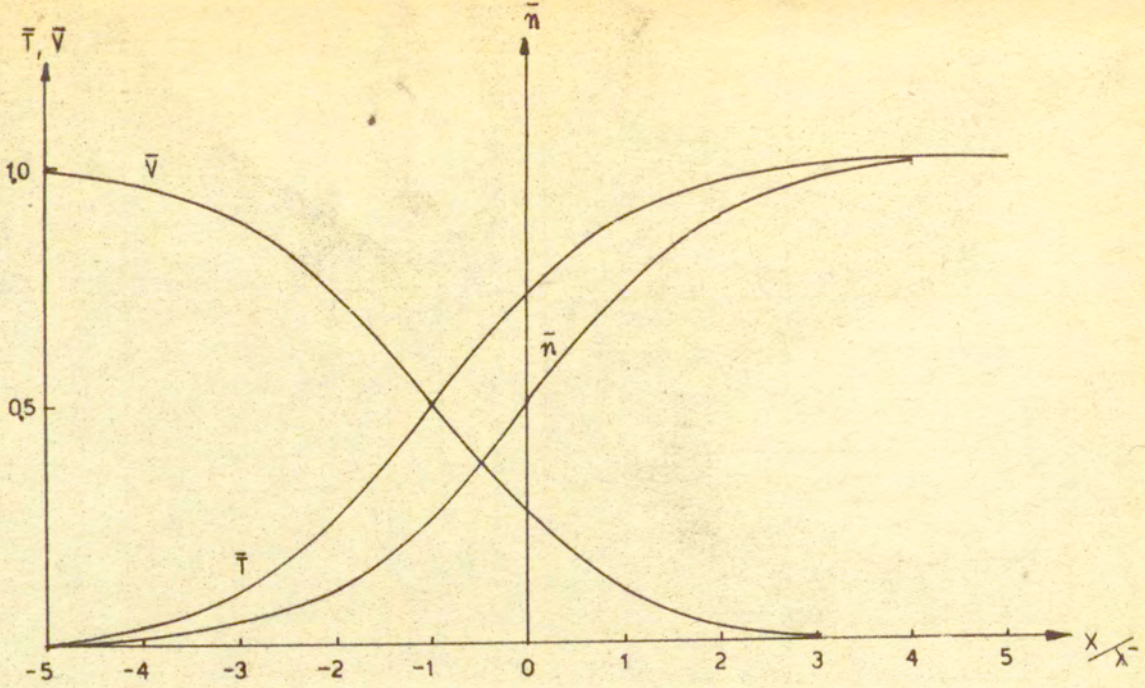

Fig. 7. The shock wave structure in monatomic gas. The distribution curves for reduced number density, velocity and temperature. (argon, $\bar{M} = 2.5$, Lennard-Jones (6-12) potential).

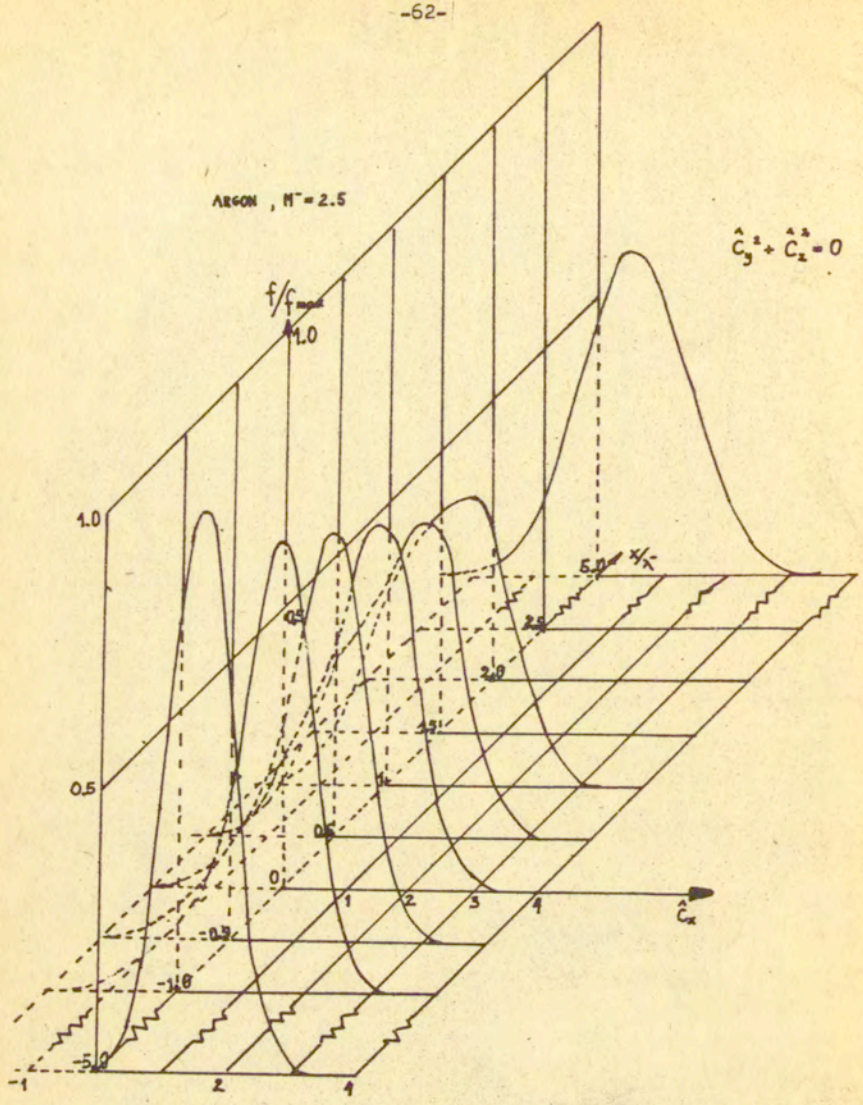

Fig. 8. The velocity distribution function within the shock wave in argon ($M^- = 2.5$); The normalized distribution function versus the dimensionless velocity component $\hat{C}_x$ and $\frac{x}{\lambda}$ (for $\hat{C}_y^2 + \hat{C}_z^2 = 0$)

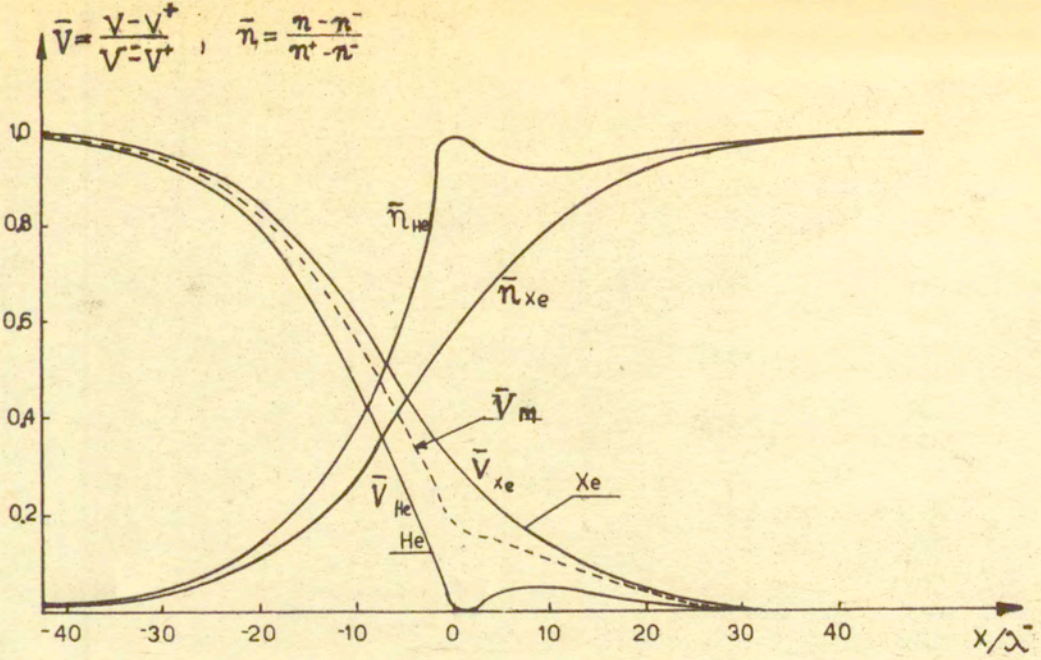

Fig. 9a. The shock wave structure in helium-xenon mixture ($M^- = 1.5$, $W_{Xe} = 0.06$); Lennard-Jones (6-12) potential model; The distribution curves for the reduced velocity and number density of both components and the mixture.

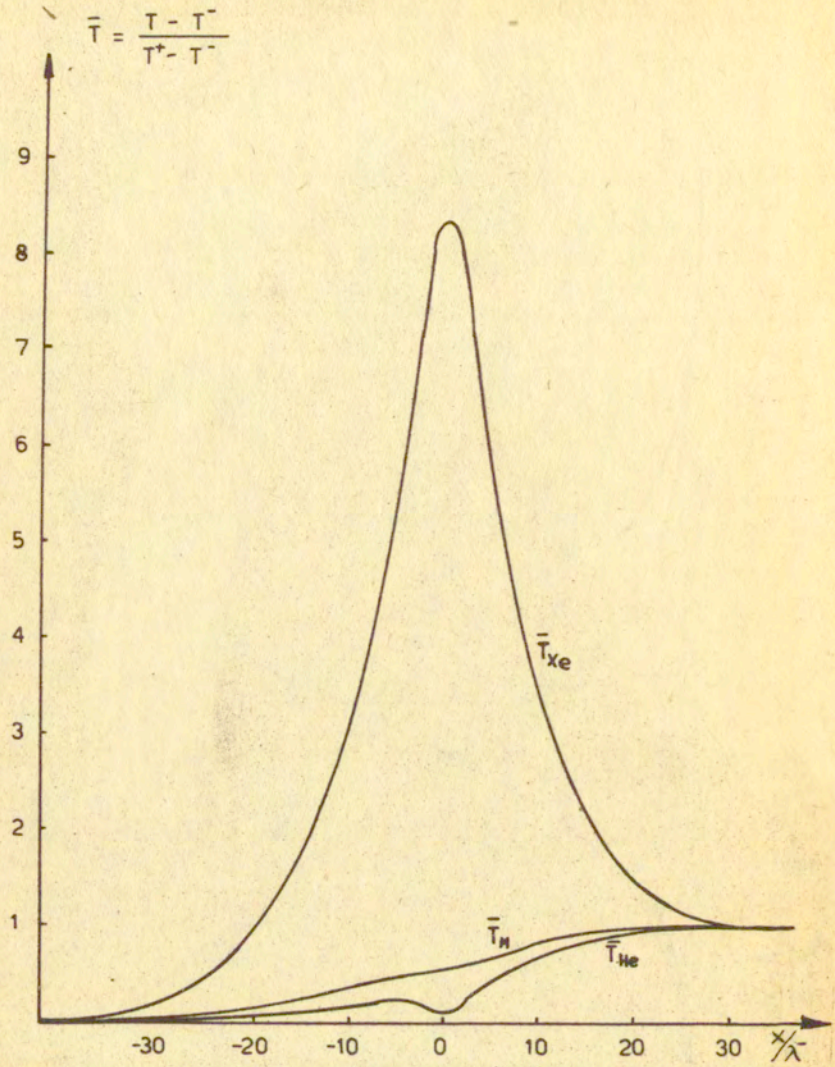

Fig.9b,c The shock wave structure in helium-xenon mixture ($M^- = 1.5$, $w_{Xe} = 0.06$); Lennard-Jones (6-12) potential. The distributions of helium, xenon and mixture temperatures.

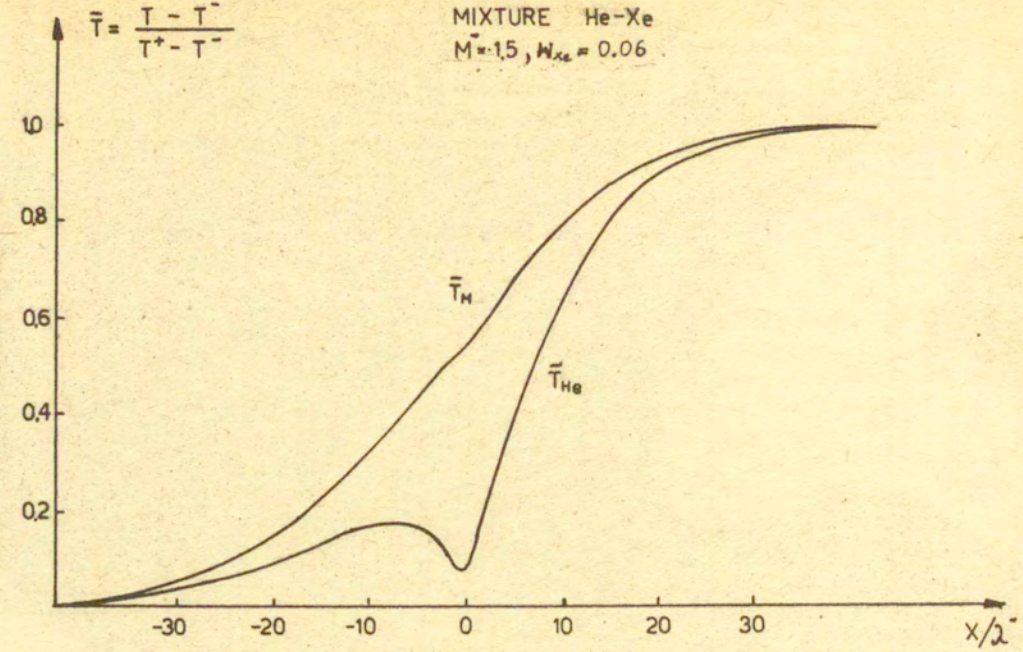

Fig. 9c

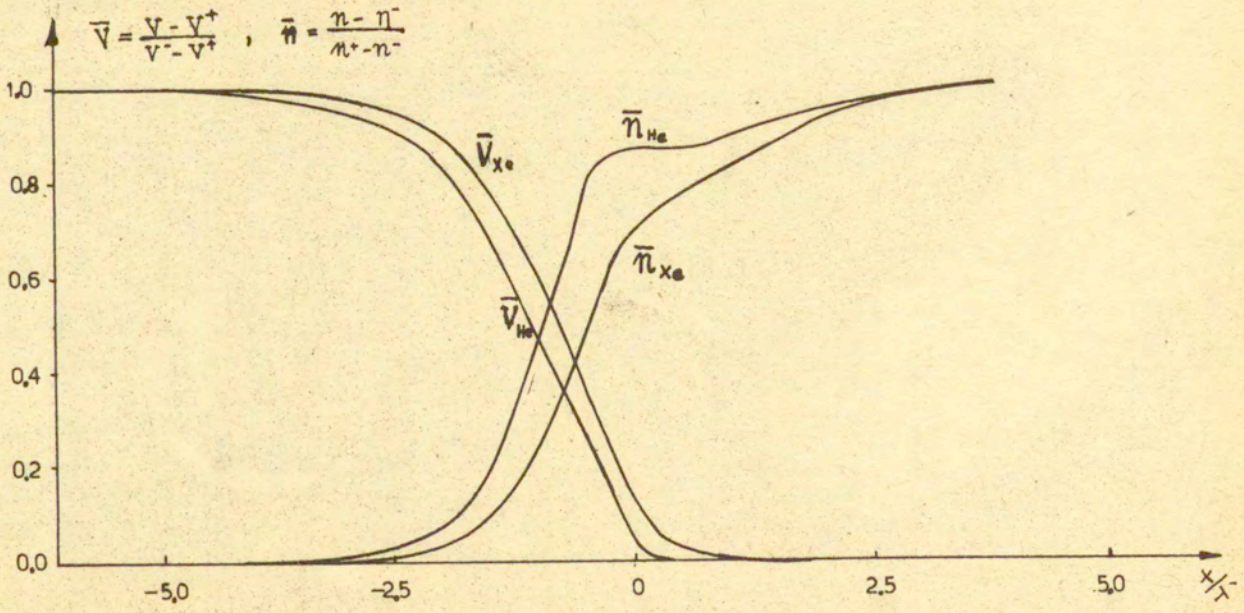

Fig. 10a. The shock wave structure in helium-xenon mixture ($M^- = 2.5$; $W_{Xe} = 0.06$); the Lennard-Jones (6-12) potential model; The distributions of the reduced velocity and number density for both components.

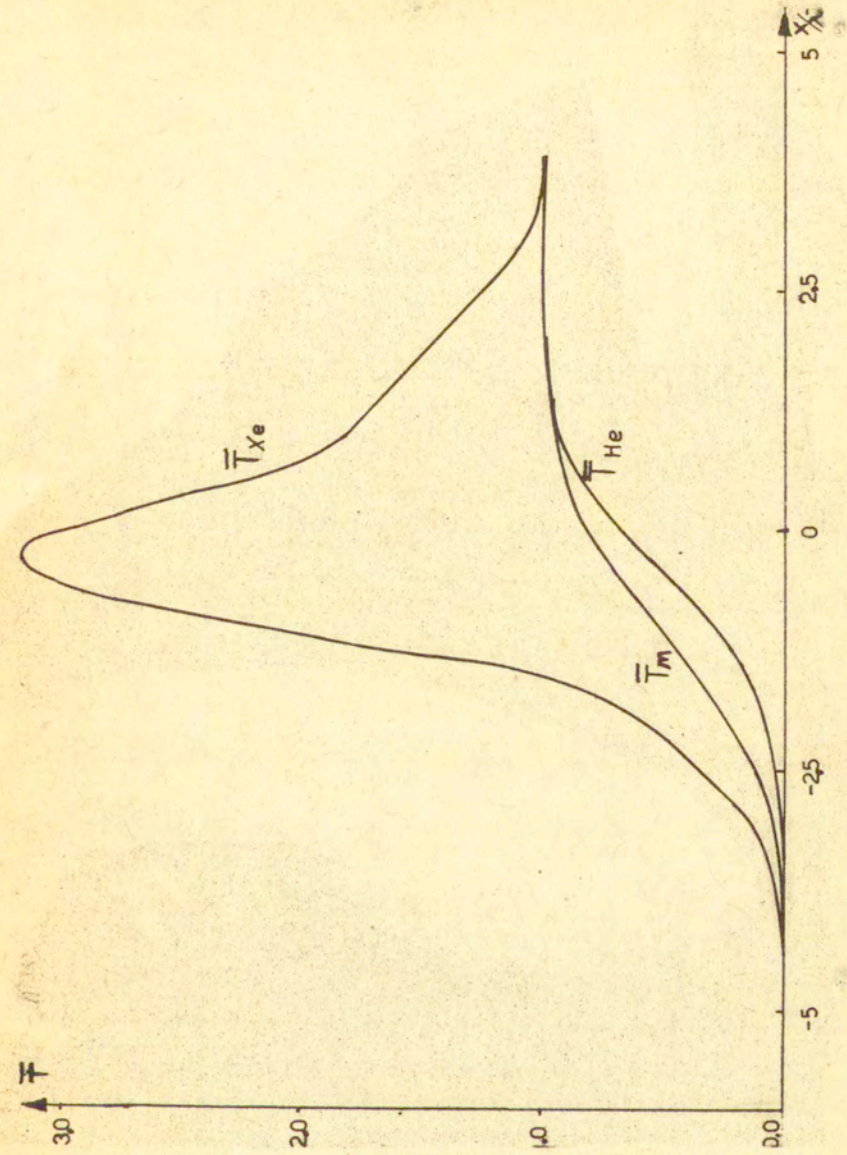

Fig. 10b. The shock wave structure in helium-xenon mixture ($M^- = 2.5$, $W_{Xe} = 0.06$); Lennard-Jones (6-12) potential model; The distribution of the reduced temperatures within the shock wave.

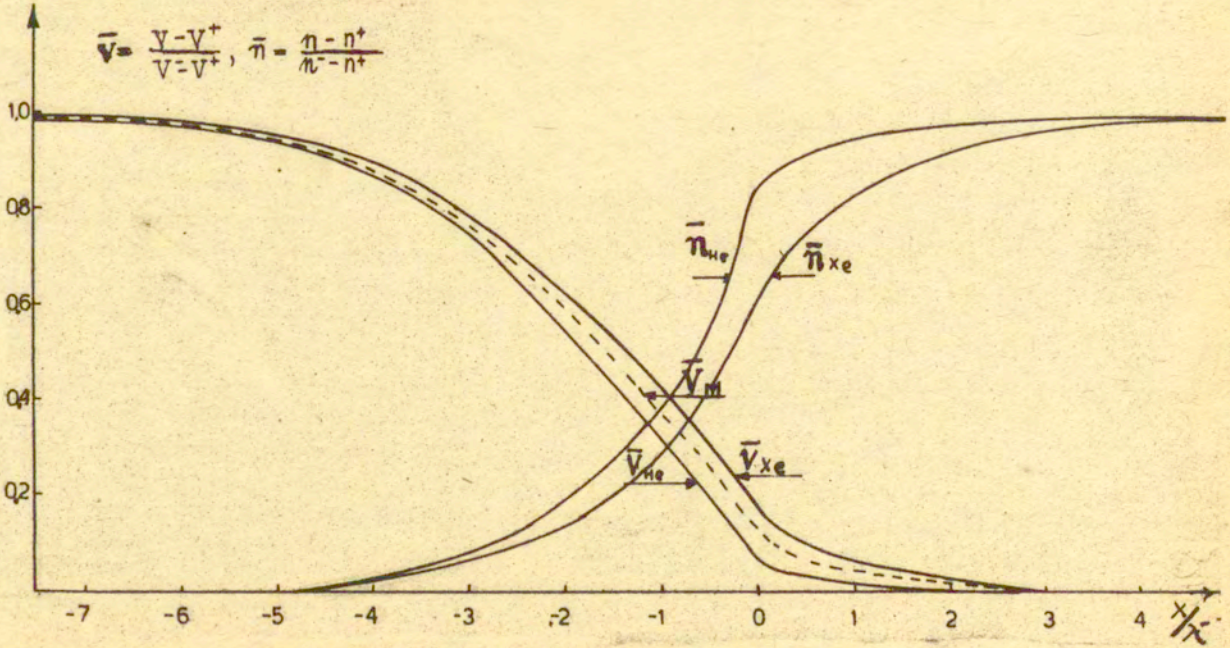

Fig. 11a. The shock wave structure in helium-xenon mixture ($M^- = 4.4$, $W_{Xe} = 0.06$); Lennard-Jones (6-12) potential; The distributions of the reduced velocities and number densities for both components.

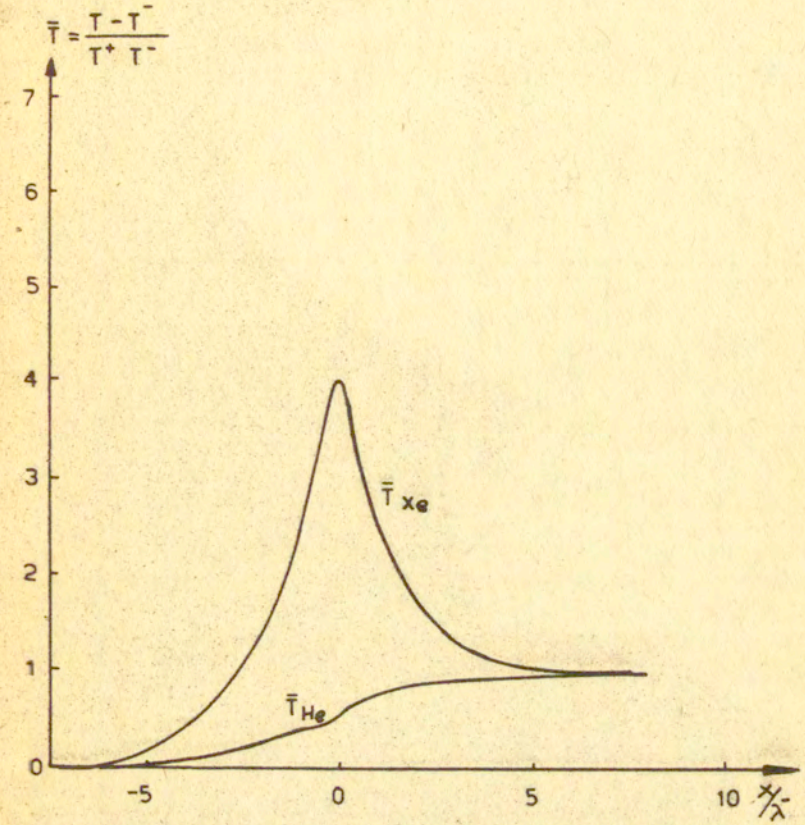

Fig. 11b,c. The shock wave structure in helium-xenon mixture ($M^- = 4.4$, $W_{Xe} = 0.06$); Lennard-Jones (6-12) potential. The distributions of the reduced temperatures for both components and mixture.

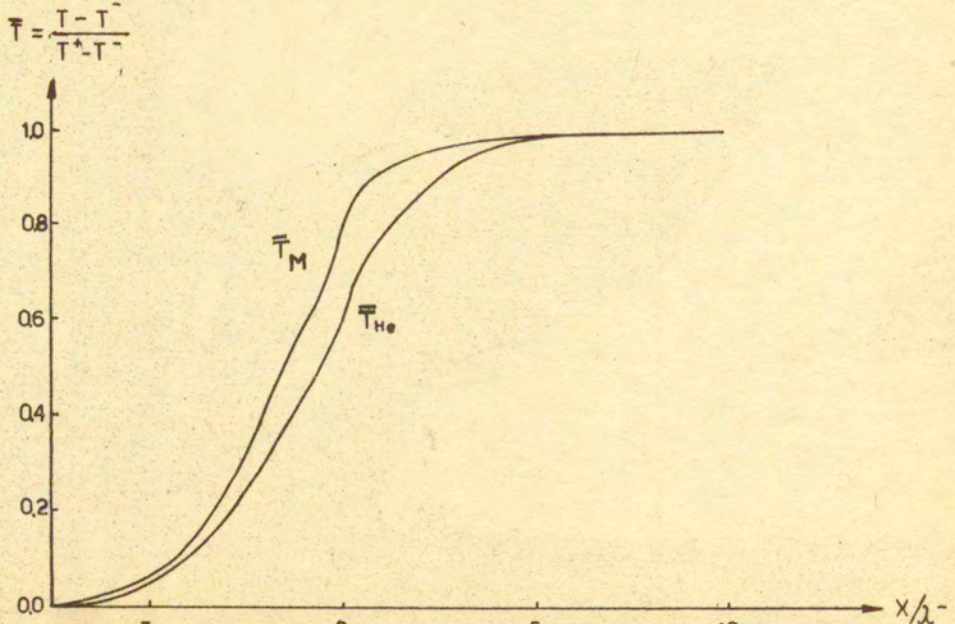

Fig. 11c

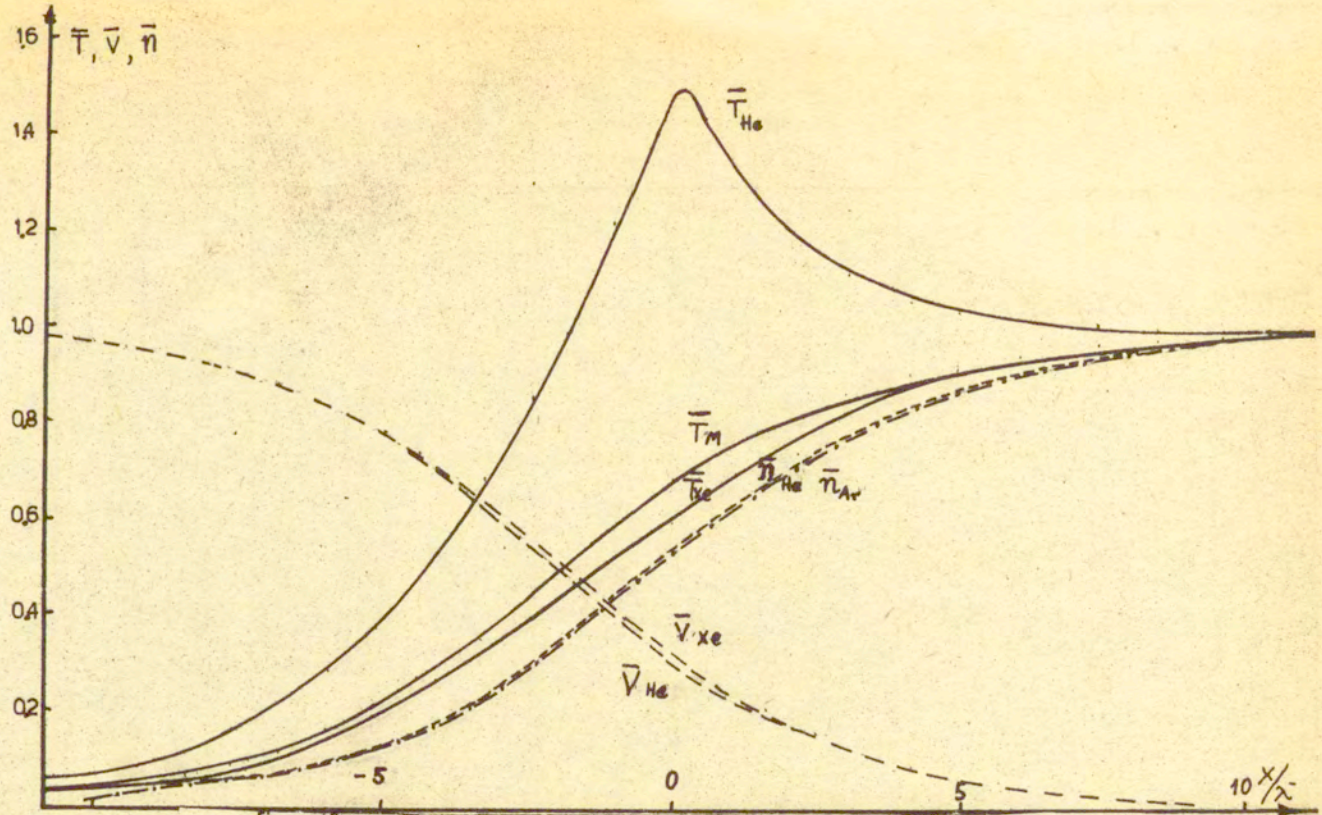

Fig. 12. The shock wave structure in helium-argon mixture ($M^- = 1.6$, $W_{Ar} = 0.05$); Lennard-Jones (6-12) potential. The distributions of the reduced number densities, velocities and temperatures for both components within the shock wave.

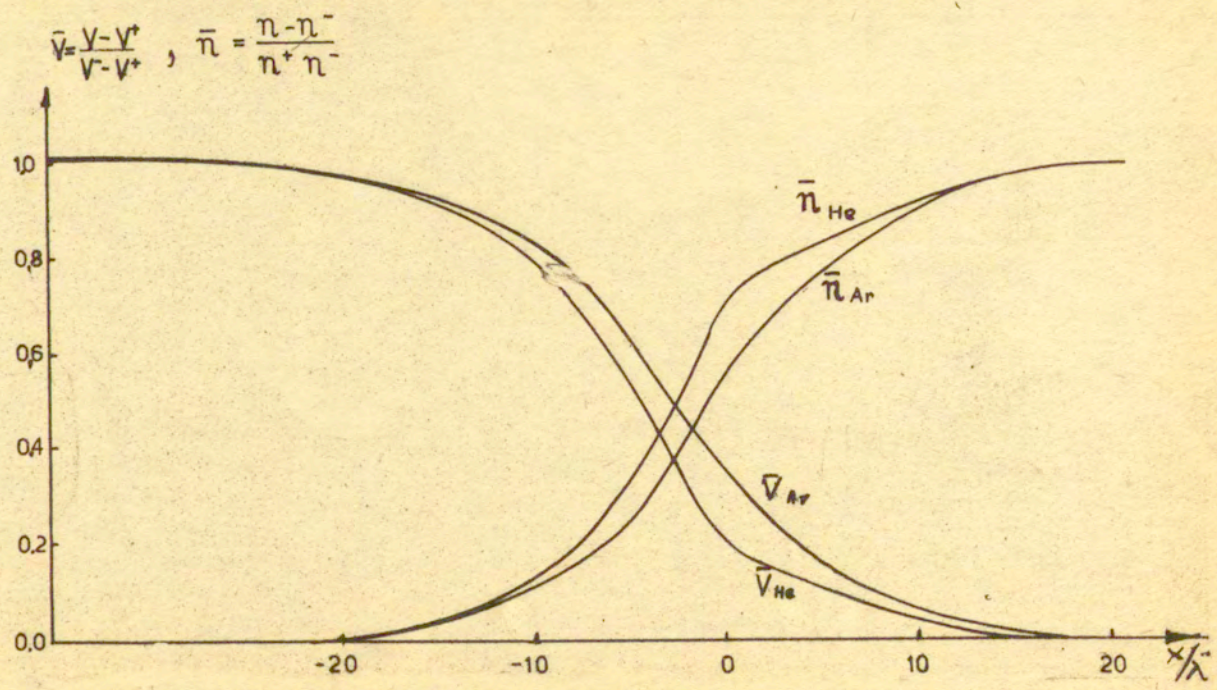

Fig. 13a. The shock wave structure in helium-argon mixture ($M^- = 1.6$, $W_{Ar} = 0.3$); Lennard-Jones (6-12) potential. The distributions of the reduced velocity and number density for helium and argon components.

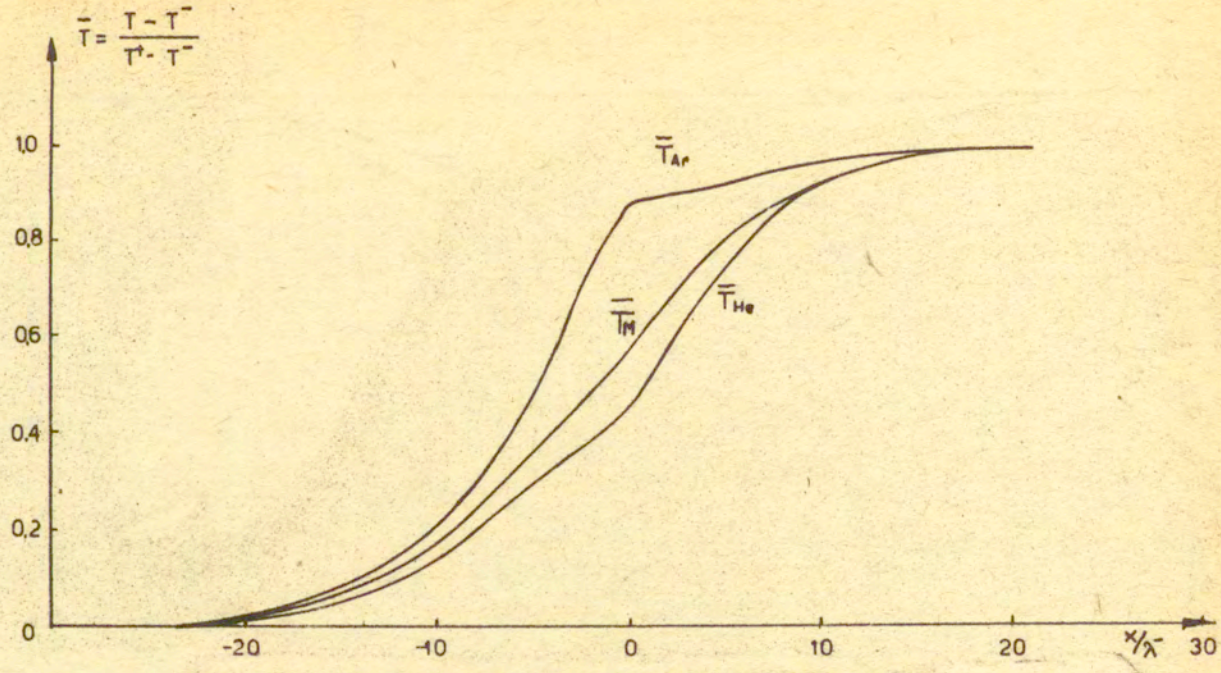

Fig. 136. The shock wave structure in helium-argon mixture ($M^- = 1.6$; $W_{Ar} = 0.3$); Lennard-Jones (6-12) potential. The distributions of the reduced temperatures.

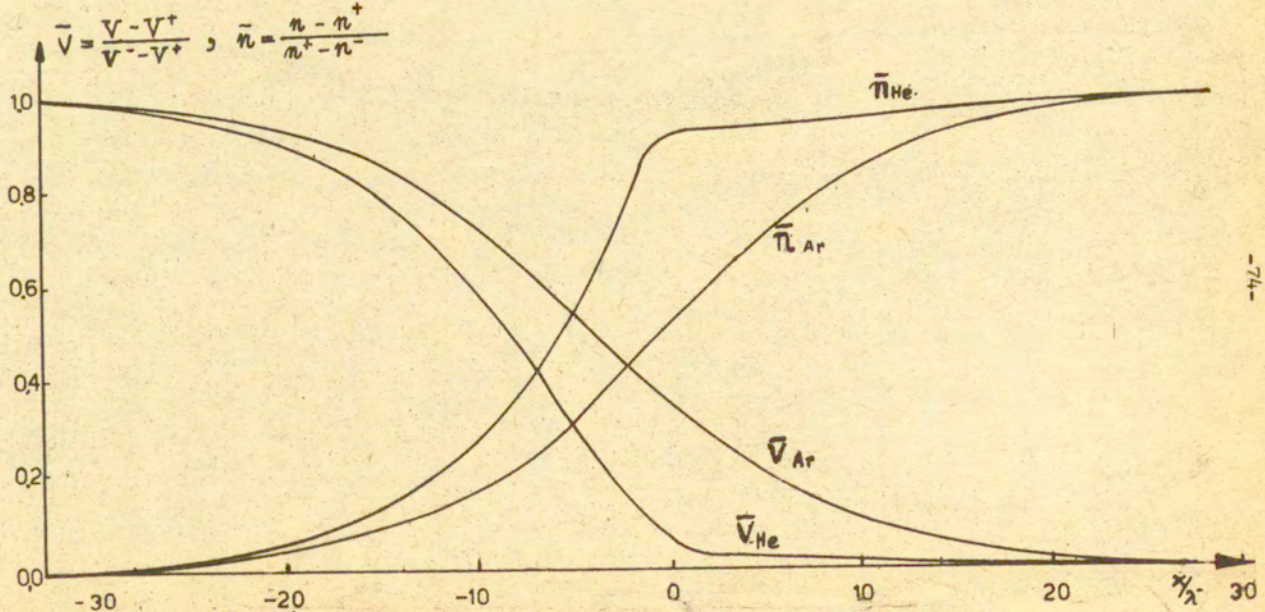

Fig. 14a. The shock wave structure in helium-argon mixture ($M^- = 1.6$, $W_{Ar} = 0.5$); Lennard-Jones (6-12) potential. The distributions of the reduced velocities and number densities for both components.

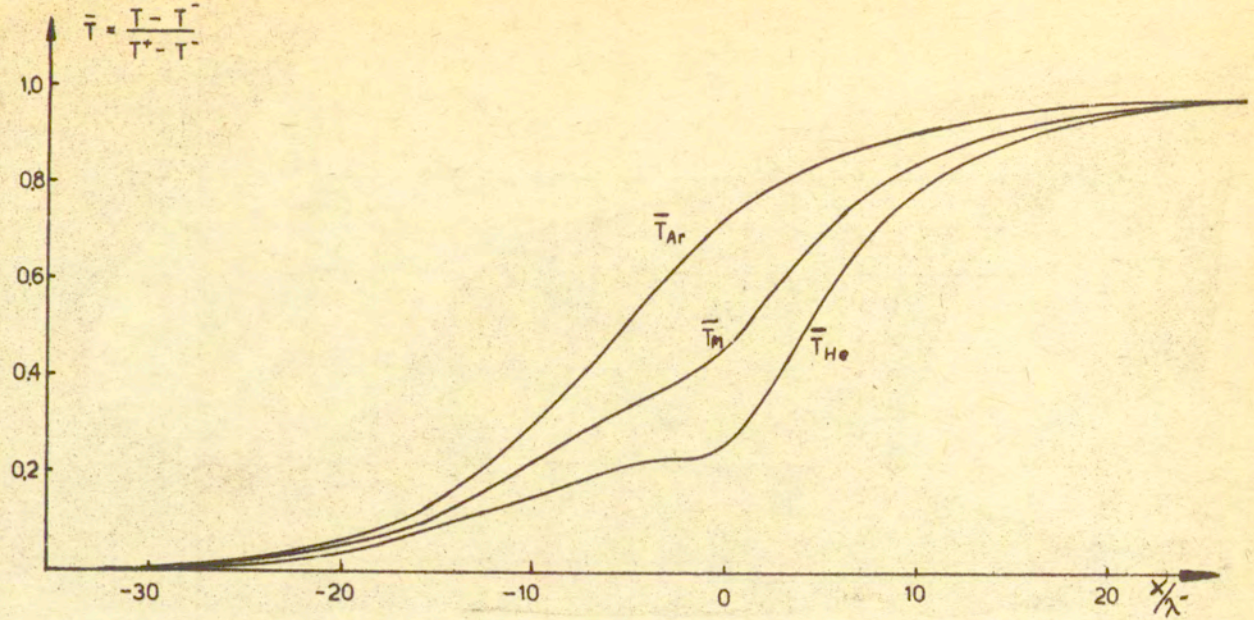

Fig. 14b. The shock wave structure in helium-argon mixture. ($M^- = 1.6$, $W_{Ar} = 0.5$); Lennard-Jones (6-12) potential. The distributions of the reduced temperatures for both components and the mixture.

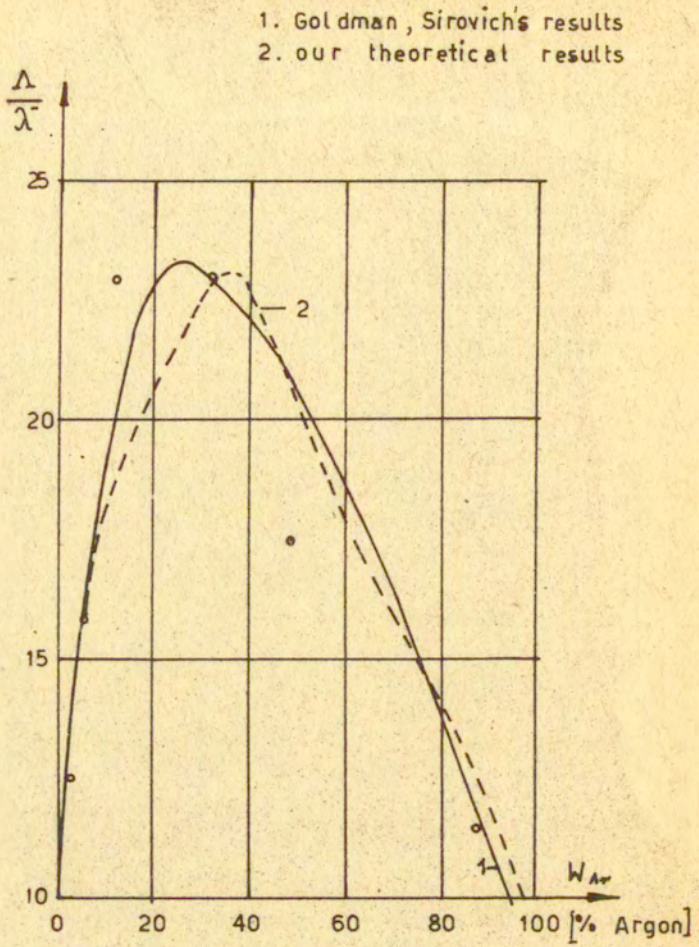

Fig.15. The comparison between experimental data (o-Center's experimental results) and the results obtained by Goldman, Sirovich [69] (curve 1) and in this work (curve 2).

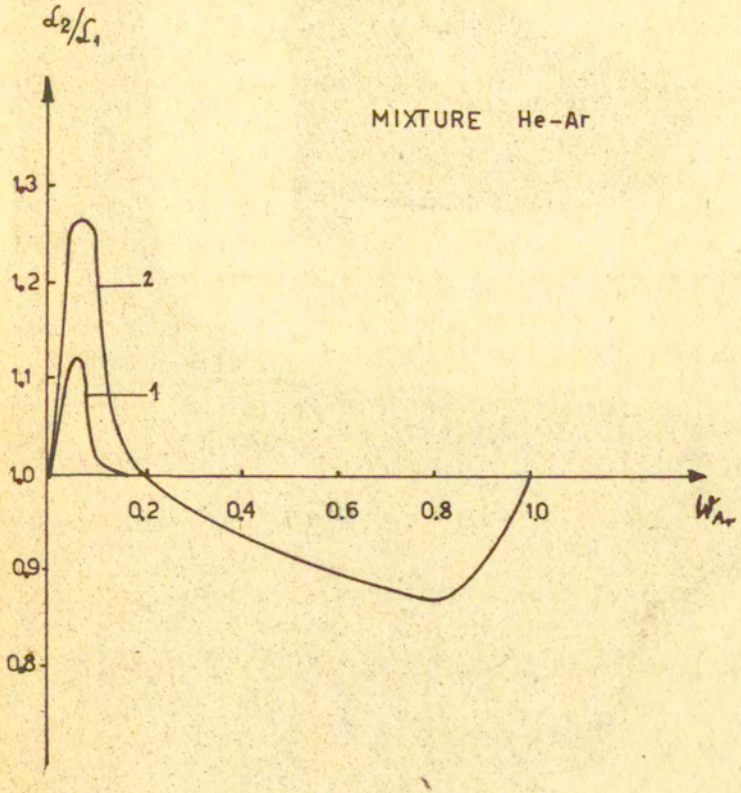

Fig. 16. The dependence of asymmetry coefficients a_3 on argon mole fraction W_{Ar} (helium-argon mixture) 1 - $M^- = 1.6$, 2 - $M^- = 3$.

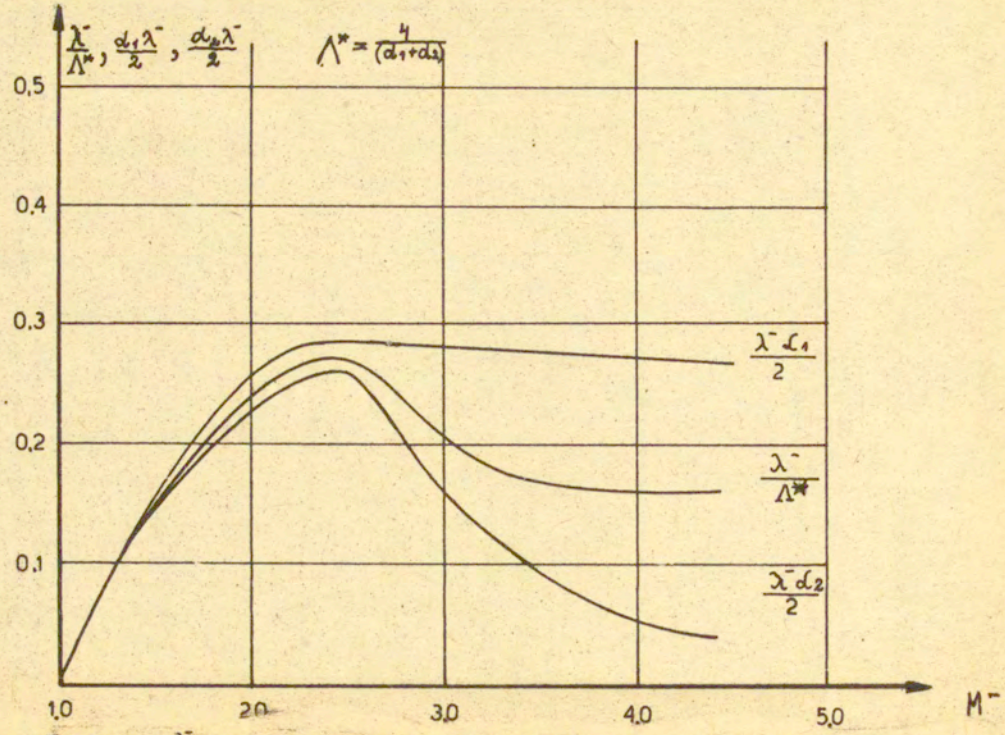

Fig. 17. $\frac{\lambda^-}{\Lambda^*}$ versus M^- (α_1, α_2 - relaxation parameters) - - helium-xenon mixture, ^{2} (W_{Xe} = 0.06, L-J (6-12) potential).

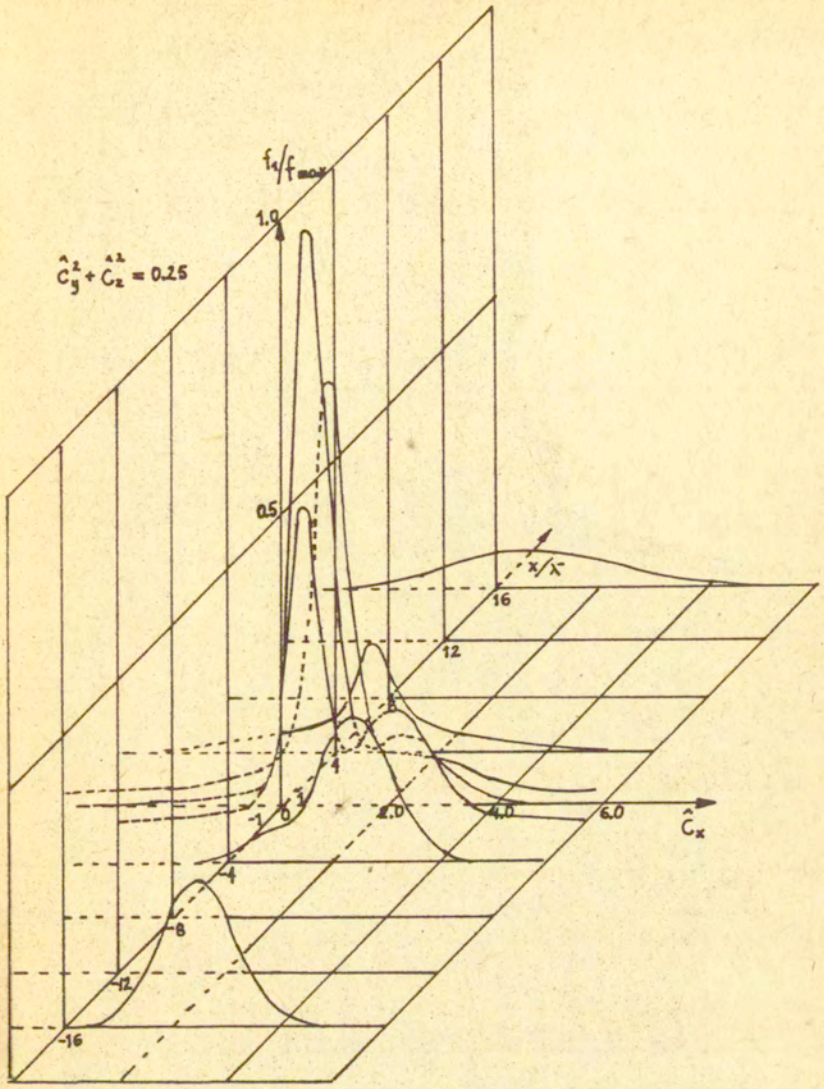

Fig. 18. The normalized velocity distribution function of light component within the shock wave (helium-xenon mixture), (M_1 = 4.4, N_{Xe} = 0.06); (Lennard-Jones (6-12) potential model); $\hat{C}_y^2 + \hat{C}_z^2 = 0.25$

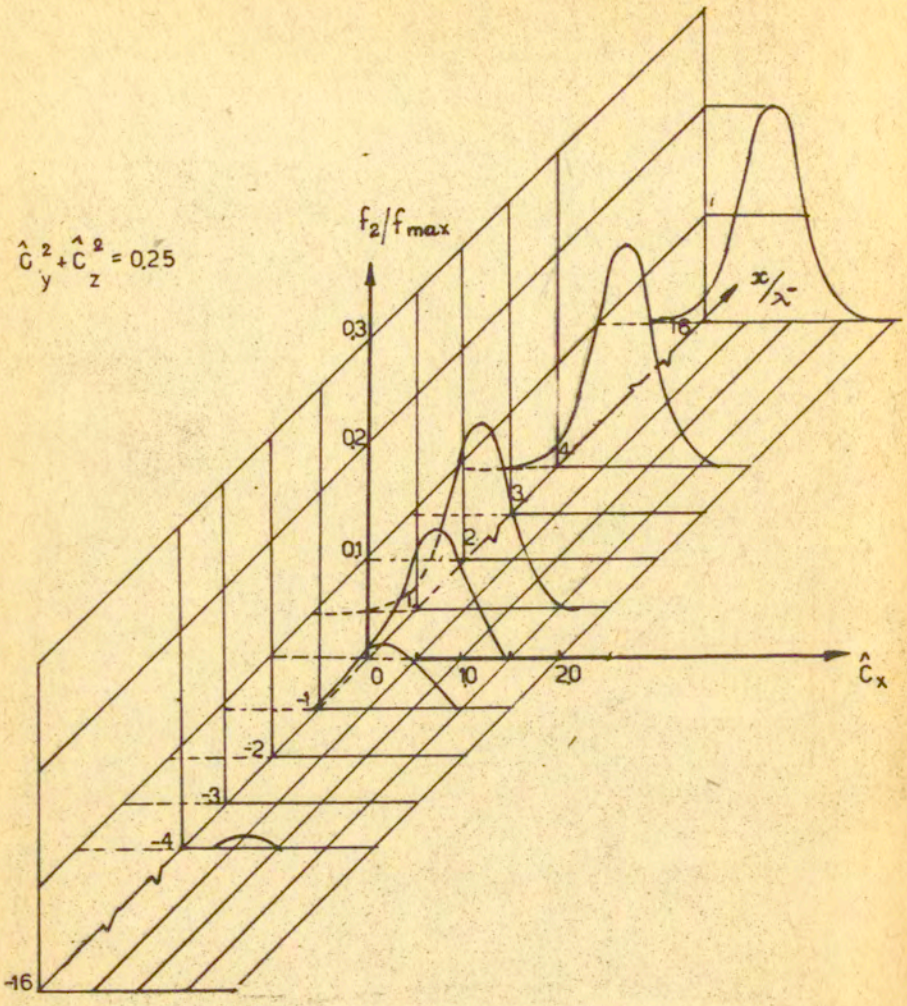

Fig. 19. The distribution of the normalized velocity distribution function of heavy component within the shock wave, in helium-xenon mixture ($M^- = 4.4$, $w_{Xe} = 0.06$, Lennard-Jones (6-12) potential model); $\hat{C}_y^2 + \hat{C}_z^2 = 0.25$

$$\delta_{glob} = \frac{S_{glob}}{2\left[\int dx \left\{ \left[\int d^{3}\bar{c} \left[\chi_1(f_1, f_2) \right] \right]^2 + \left[\int d^{3}\bar{c} \left[\chi_2(f_1, f_2) \right] \right]^2 \right\}}$$

δ_{glob} where $S_{glob} = S$ [2,4]

and $$S_{lok} = \sum_{i=1}^{N} \left(\left[\underline{\dot{c}} \, \mathrm{grad} f_i - \sum_{j=1}^{N} \chi_{ij} \right]^2 d^{3}\bar{c} \right)$$

and where $\chi_1 = \chi_{11} + \chi_{12}$; $\chi_2 = \chi_{21} + \chi_{22}$

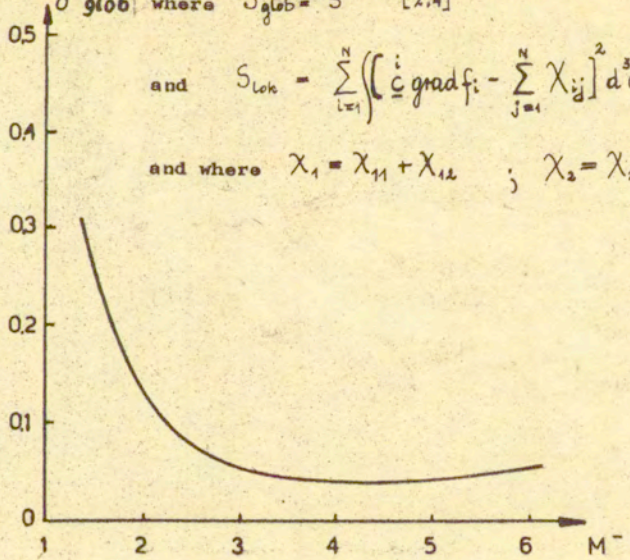

$$S_{lok\,max} = \frac{S_{lok}(0)}{2\left[\int \left\{ \chi_1(f_1, f_2) \right\}^2 d^{3}\bar{c} + \int \left\{ \chi_2(f_1, f_2) \right\}^2 d^{3}\bar{c} \right]}$$

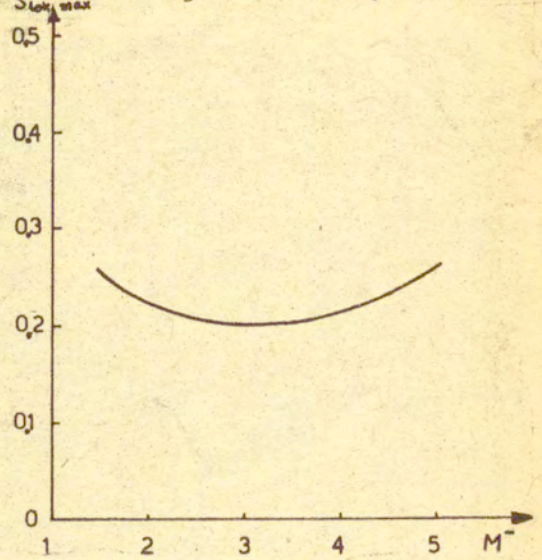

Fig. 20 a,b. The accuracy of the method. The dependence of the global error on M^-. The dependence of maximum local error on M^-.

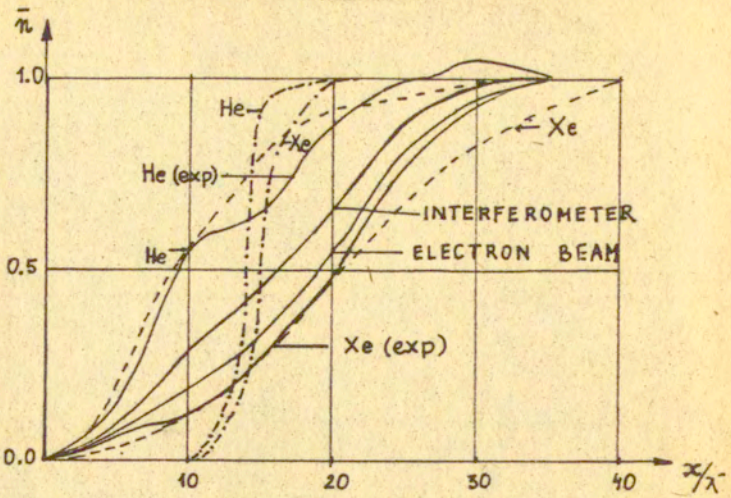

Fig.21 The comparison of our results with experiment and other theoretical results; $\bar{n}(x/\lambda_-)$ distribution within the shock wave —experiment [1,2]; ----Płatkowski's results, -·-·-·- our results ($M^- = 4.4$, $W_{Xe} = 0.06$).